PUBLISHED VERSION

Deka, M.; Steuer, T.; Doi, T.; Dong, Shao-Jing; Draper, Terrence; Liu, K. F.; Mathur, Nilmani; Thomas, Anthony William
Moments of nucleon's parton distribution for the sea and calence quarks from lattice QCD
Physical Review. D, 2009; 79(9):094502

©2009 American Physical Society

http://link.aps.org/doi/10.1103/PhysRevD.79.094502

PERMISSIONS

http://publish.aps.org/authors/transfer-of-copyright-agreement

"The author(s), and in the case of a Work Made For Hire, as defined in the U.S. Copyright Act, 17 U.S.C.

§101, the employer named [below], shall have the following rights (the "Author Rights"):

[...]

3. The right to use all or part of the Article, including the APS-prepared version without revision or modification, on the author(s)' web home page or employer's website and to make copies of all or part of the Article, including the APS-prepared version without revision or modification, for the author(s)' and/or the employer's use for educational or research purposes."

31st May 2013

http://hdl.handle.net/2440/67510

Moments of nucleon's parton distribution for the sea and valence quarks from lattice QCD

M. Deka,[1,*] T. Streuer,[2] T. Doi,[1] S. J. Dong,[1] T. Draper,[1] K. F. Liu,[1] N. Mathur,[3] and A. W. Thomas[4]

[1]*Department of Physics and Astronomy, University of Kentucky, Lexington, Kentucky 40506, USA*
[2]*Institute for Theoretical Physics, University of Regensburg, 93040 Regensburg, Germany*
[3]*Department of Theoretical Physics, Tata Institute of Fundamental Research, Mumbai 40005, India*
[4]*Thomas Jefferson National Accelerator Facility, Newport News, Virginia 23606, USA*

(Received 11 November 2008; published 12 May 2009)

We extend the study of lowest moments, $\langle x\rangle$ and $\langle x^2\rangle$, of the parton distribution function of the nucleon to include those of the sea quarks; this entails a disconnected insertion calculation in lattice QCD. This is carried out on a $16^3 \times 24$ quenched lattice with Wilson fermion. The quark loops are calculated with Z_2 noise vectors and unbiased subtractions, and multiple nucleon sources are employed to reduce the statistical errors. We obtain 5σ signals for $\langle x\rangle$ for the u, d, and s quarks, but $\langle x^2\rangle$ is consistent with zero within errors. We provide results for both the connected and disconnected insertions. The perturbatively renormalized $\langle x\rangle$ for the strange quark at $\mu = 2$ GeV is $\langle x\rangle_{s+\bar{s}} = 0.027 \pm 0.006$ which is consistent with the experimental result. The ratio of $\langle x\rangle$ for s vs u/d in the disconnected insertion with quark loops is calculated to be 0.88 ± 0.07. This is about twice as large as the phenomenologically fitted $\frac{\langle x\rangle_{s+\bar{s}}}{\langle x\rangle_{\bar{u}}+\langle x\rangle_{\bar{d}}}$ from experiments where $\bar{u}$ and $\bar{d}$ include both the connected and disconnected insertion parts. We discuss the source and implication of this difference.

DOI: 10.1103/PhysRevD.79.094502 PACS numbers: 11.15.Ha, 11.30.Rd, 12.38.Gc, 13.60.Hb

I. INTRODUCTION

Recently, there has been a good deal of interest in the study of sea quarks, both in theory and experiment. In such studies, strange quarks play an important role in observables involving sea quarks. For more than a decade, intensive studies have been made in measuring and understanding the strangeness contribution to the nucleon spin [1], the electromagnetic form factors [2–5], the strangeness condensate [6], and the parton distribution function in the nucleon [7–9]. Another important aspect of studying strangeness content is to address the issue of the *NUTEV anomaly*. The NUTEV experiment ($\nu + N \rightarrow \mu + X$) [10], which measures the Weinberg angle or weak mixing angle, an important parameter in the Standard Model of particle physics, finds a value which is 3 standard deviations away from the world average value. One suggestion to explain this discrepancy is the asymmetry in strange and antistrange parton distribution [11,12], a nonperturbative effect. Attempts by various theoretical models to calculate the asymmetry give inconsistent results (sometimes with completely opposite signs) [12–16]. Also, phenomenological extractions by CTEQ and NUTEV [17,18] for leading order and next-to-leading order give different results. Lattice QCD can assess this asymmetry from first principles in terms of $\langle x^2\rangle_{s-\bar{s}}$ to address whether it is strange or antistrange which is leading in large x. This information will be helpful to constrain and analyze the experimental data. Similarly, the first moment of the strange parton distribution, $\langle x\rangle_{s+\bar{s}}$ is not well known. It ranges between 0.018 and 0.04 from the fitting of parton distribution functions to experiments [8].

In the present work, we will study the first and second moments of quark distribution for up, down and strange quarks. The first moment provides the measure of the symmetric contribution from parton and antiparton distributions ($q + \bar{q}$) and the second moment provides the measure of the asymmetry in parton and antiparton distributions ($q - \bar{q}$). These moments have contributions both from connected and disconnected insertions for up and down quarks and only disconnected insertion for strange quarks. Since lattice calculations on connected insertions, for the first and second moments, have been done before, this work is going to focus mainly on disconnected insertion contributions (particularly for strange quarks) to the first and second moments, which has not been attempted in lattice QCD.

This paper is organized as follows. We give the formalism and lattice operators in Sec. II. The disconnected insertion calculation is presented in Sec. III. The perturbative renormalization is given in Sec. IV. Sec. V presents numerical parameters and error studies of the noise estimate. The results for both the disconnected insertions and connected insertions are given in Sec. VI. Finally, we offer a conclusion and some discussion in Sec. VII. Some details of the three-point correlation functions are given in the Appendices.

II. FORMALISM

In deep inelastic scattering [19], it is useful to consider and analyze the moments of the structure function via the operator product expansion (OPE) where, in the limit of distance $x \rightarrow 0$ or equivalently $q \rightarrow \infty$, the product of two

*mpdeka@pa.uky.edu

 © 2009 The American Physical Society

operators can be expanded in terms of local operators

$$\lim_{x\to 0}\mathcal{O}_i(x)\mathcal{O}_j(0) = \sum_k c_{ijk}(x,\mu)\mathcal{O}_k(\mu), \tag{1}$$

where c's are the Wilson coefficients.

The leading term for such an expansion has the lowest *twist*, $t = 2$. For unpolarized structure functions with vector currents J^μ, the twist-two operators for quarks have the bilinear form

$$\mathcal{O}_f^{(n)\mu_1\cdots\mu_n} = \bar{\psi}_f\gamma^{\{\mu_1}(i\overleftrightarrow{\mathcal{D}})^{\mu_2}\cdots(i\overleftrightarrow{\mathcal{D}})^{\mu_n\}}\psi_f - \text{traces}, \tag{2}$$

where ψ_f denotes the quark field operator for the flavor f, $\overleftrightarrow{\mathcal{D}} = \frac{1}{2}(\vec{\mathcal{D}} - \overleftarrow{\mathcal{D}})$, and $\{\cdots\}$ stands for symmetrization of the indices, μ's. The subtracted trace terms are proportional to $g^{\mu_i\mu_j}$, so that the operator is traceless on all pairs of indices.

In the leading twist, the moments of structure functions F_1 and F_2 can be written as

$$\begin{aligned} 2\int_0^1 dx x^{n-1}F_1(x,Q^2) &= \sum_f c_f^{1,n}(\mu^2/Q^2, g(\mu))A_f^n(\mu), \\ \int_0^1 dx x^{n-2}F_2(x,Q^2) &= \sum_f c_f^{2,n}(\mu^2/Q^2, g(\mu))A_f^n(\mu), \\ &\quad (\text{for } n \geq 2) \end{aligned} \tag{3}$$

where A_f^n is defined through the forward matrix elements

$$\langle P|\mathcal{O}_f^{(n)\mu_1\cdots\mu_n}|P\rangle = 2A_f^n P^{\mu_1}\cdots P^{\mu_n} - \text{traces}. \tag{4}$$

In the parton model, A_f^n has the interpretation as the $(n-1)$th moment of the momentum fraction carried by the quarks with flavor f at some scale μ, i.e.

$$A_f^n(\mu) = \int_0^1 dx x^{n-1}[f(x) + (-1)^n\bar{f}(x)], \tag{5}$$

where $f(x)$ is the quark distribution function and $\bar{f}(x)$ is the antiquark distribution function for the flavor f. We see that the first moment ($n = 2$) has the symmetric combination of the quark and antiquark distribution and the second moment ($n = 3$), due to the interference between the vector and axial-vector part of the weak interaction current, has the asymmetric combination of the quark and antiquark distribution. Our goal is to compute the first and second moments for up, down, and strange quarks.

A. Lattice operators

Lattice calculations are carried out in Euclidean path-integral. Thus, we need to transform the twist-two operators from Minkowski space to Euclidean space. Following the convention [20,21]

$$\begin{aligned} \gamma^{(M)0} &\to \gamma_4^{(E)}, \qquad \gamma^{(M)j} \to i\gamma_j^{(E)}, \\ iD^{(M)0} &\to -D_4^{(E)}, \qquad iD^{(M)j} \to -iD_j^{(E)}, \end{aligned} \tag{6}$$

with the γ matrices defined as

$$\begin{aligned} \{\gamma_\mu,\gamma_\nu\} = 2\delta_{\mu\nu}, \qquad \gamma_5 = \gamma_1\gamma_2\gamma_3\gamma_4, \\ \sigma_{\mu\nu} = \frac{1}{2i}[\gamma_\mu,\gamma_\nu], \end{aligned} \tag{7}$$

we can transform the twist-two operators in Eq. (2) to its Euclidean counterpart by using the notation [22]

$$\mathcal{O}_{(f)\mu_1\cdots\mu_n}^{(n)(E)} \leftarrow h_{\mu_1\nu_1}d_{\mu_2\nu_2}\cdots d_{\mu_n\nu_n}\mathcal{O}_f^{(M)(n)\nu_1\cdots\nu_n}, \tag{8}$$

where $h_{\mu\nu} = \text{diag}(i,i,i,1)$ and $d_{\mu\nu} = \text{diag}(-1,-1,-1,i)$. We have also set $a^{(M)0} = a^{(M)4}$ for any four vector, a. From now on we will consider Euclidean operators only and drop the superscript, E. Since the Euclidean signature is $(++++)$, the subtracted trace terms are proportional to $\delta_{\mu_i\mu_j}$. To be specific, we use the Pauli-Sakurai γ matrix convention in our calculation.

We discretize our current operators by using the following relations for right and left derivatives in lattice [23]

$$\begin{aligned} \vec{D}_\mu\psi^L(x) = \frac{1}{2a}[&U_\mu(x)\psi^L(x+a_\mu) \\ &- U_\mu^\dagger(x-a_\mu)\psi^L(x-a_\mu)], \end{aligned} \tag{9}$$

$$\begin{aligned} \bar{\psi}^L(x)\overleftarrow{D}_\mu = \frac{1}{2a}[&\bar{\psi}^L(x+a_\mu)U_\mu^\dagger(x) \\ &- \bar{\psi}^L(x-a_\mu)U_\mu(x-a_\mu)], \end{aligned} \tag{10}$$

where a is the lattice spacing. For example, the two-index operator, $\mathcal{O}_{\mu\nu}$, can be written as

$$\begin{aligned} \mathcal{O}_{\mu\nu}(x) = \frac{\lambda}{8a}[&\bar{\psi}^{(f)}(x)\gamma_\mu U_\nu(x)\psi^{(f)}(x+a_\nu) - \bar{\psi}^{(f)}(x)\gamma_\mu U_\nu^\dagger(x-a_\nu)\psi^{(f)}(x-a_\nu) + \bar{\psi}^{(f)}(x-a_\nu)\gamma_\mu U_\nu(x-a_\nu)\psi^{(f)}(x) \\ &- \bar{\psi}^{(f)}(x+a_\nu)\gamma_\mu U_\nu^\dagger(x)\psi^{(f)}(x) + \bar{\psi}^{(f)}(x)\gamma_\nu U_\mu(x)\psi^{(f)}(x+a_\mu) - \bar{\psi}^{(f)}(x)\gamma_\nu U_\mu^\dagger(x-a_\mu)\psi^{(f)}(x-a_\mu) \\ &+ \bar{\psi}^{(f)}(x-a_\mu)\gamma_\nu U_\mu(x-a_\mu)\psi^{(f)}(x) - \bar{\psi}^{(f)}(x+a_\mu)\gamma_\nu U_\mu^\dagger(x)\psi^{(f)}(x)], \end{aligned} \tag{11}$$

where $\lambda = -i$ for $\mu = 4$, $\nu = 1,2,3$; $\lambda = +1$ for $\mu = \nu = 1,2,3$ and $\lambda = -1$ for $\mu = \nu = 4$. Similar expressions can be obtained for the three-index operators.

Since in lattice QCD the continuous space-time space is described on a four-dimensional cubic lattice, the $O(4)$ group in the continuum reduces to the hypercubic group $H(4)$ [24,25]. This implies that operators belonging to irreducible

representations of $O(4)$ may transform in a reducible way under $H(4)$. This will allow them to mix with lower dimensional operators under renormalization. In order to avoid such mixing, it is suggested to adopt the following combination of operators which have minimal mixing (or no mixing) [26–29]. For two-index operators (for $\langle x \rangle$), we choose $\mathcal{O}_{4i}(i = 1, 2, 3)$ and $\tilde{\mathcal{O}}_{44} = \mathcal{O}_{44} - \frac{1}{3}(\mathcal{O}_{11} + \mathcal{O}_{22} + \mathcal{O}_{33})$ which does not suffer from any mixing [26,28]. The best choice for three-index operator (for $\langle x^2 \rangle$) is $\tilde{\mathcal{O}}_{4ii} = \mathcal{O}_{4ii} - \frac{1}{2}(\mathcal{O}_{4jj} + \mathcal{O}_{4kk})$, where $i, j, k = 1, 2, 3(i \neq j \neq k)$, which still suffers from some mixing [26,29]. The matrix elements for these operators are

$$\begin{aligned} \langle P|\mathcal{O}^f_{4i}|P\rangle &= -\frac{2}{2m}\langle x\rangle_{f+\bar{f}} E P_i, \\ \langle P|\tilde{\mathcal{O}}^f_{44}|P\rangle &= \frac{2}{2m}\langle x\rangle_{f+\bar{f}} E^2, \\ \langle P|\tilde{\mathcal{O}}^f_{4ii}|P\rangle &= \frac{2}{2m}\langle x^2\rangle_{f-\bar{f}} E p_i^2, \end{aligned} \tag{12}$$

where the $2m$ factor, with m being the nucleon mass, is due to the normalization of the spinors with $\bar{u}(p, s)u(p, s') = \delta_{ss'}$.

B. Two-point and three-point correlation functions

The proton two-point function we use (with the color indices suppressed) is

$$G^{\alpha\beta}_{NN}(t, \vec{p}) = \sum_{\vec{x}} e^{-i\vec{p}.(\vec{x}-\vec{x}_0)} \langle 0|\mathrm{T}[\chi^\alpha(\vec{x}, t)\bar{\chi}^\beta(\vec{x}_0, t_0)]|0\rangle, \tag{13}$$

where t is the nucleon sink time, and $\vec{p}$ is the momentum of the nucleon. The interpolating fields [30–34] we use are

$$\chi_\gamma(x) = \epsilon_{abc}\psi^{\mathrm{T}(u)a}_\alpha(x)(C\gamma_5)_{\alpha\beta}\psi^{(d)b}_\beta(x)\psi^{(u)c}_\gamma(x), \tag{14}$$

$$\bar{\chi}_{\gamma'}(x) = -\epsilon_{def}\bar{\psi}^{(u)f}_{\gamma'}(x)\bar{\psi}^{(d)e}_\rho(x)(\gamma_5 C)_{\rho\sigma}\bar{\psi}^{\mathrm{T}(u)d}_\sigma(x), \tag{15}$$

where u and d stand for up and down quarks, respectively. $C = \gamma_2\gamma_4$, is the charge conjugation operator with the Pauli-Sakurai γ matrices. The letters, $a, b, \cdots$, stand for the color indices. The Greek letters, $\alpha, \beta, \ldots$, are the spin indices.

Since we are interested only in nucleon with $J^P = \frac{1}{2}^+$, we use the projection operator $\Gamma = \frac{1}{2}(1 + \frac{m^-}{E^{0-}_p}\gamma_4)$ [35] to eliminate the contamination from negative parity S_{11} state. Here m^- and E^{0-}_p are the mass and energy of the S_{11} state. After applying the projection operator, we get the two-point function as

$$\mathrm{Tr}[\Gamma G_{NN}(t, \vec{p})] = \frac{a^6}{(2\kappa)^3}|\phi^+|^2\frac{m^+}{E^{0+}_p}\left(1 + \frac{m^-}{E^{0-}_p}\frac{E^{0+}_p}{m^+}\right)e^{-E^{0+}_p(t-t_0)} + \sum_{\theta=+,-}\sum_{n^{(\theta)}=1}^{\infty} e^{-E^{n^{(\theta)}}_p(t-t_0)}\tilde{f}(n^{(\theta)}, \vec{p}), \tag{16}$$

where the superscript $\theta = +, -$ represents positive (negative) parity states and

$$\tilde{f}(n^{+,-}, \vec{p}) = N\Gamma^{\alpha\beta}\sum_s \langle 0|\chi^\alpha(x_0)|n^{+,-}, \vec{p}, s\rangle \times \langle n^{+,-}, \vec{p}, s|\bar{\chi}^\beta(x_0)|0\rangle, \tag{17}$$

N being the number of lattice points.

As a result, the projected two-point function with momentum $\vec{p}$ at large time separation, i.e. $t \gg t_0$, will filter out the excited states, leaving only the nucleon state remaining asymptotically

$$\mathrm{Tr}[\Gamma G_{NN}(t, \vec{p})] \xrightarrow{(t-t_0)\gg 1} \left[\frac{a^6}{(2\kappa)^3}|\phi^+|^2\frac{m^+}{E^0_p}\left(1 + \frac{m^-}{E^{0-}_p}\frac{E^{0+}_p}{m^+}\right)\right] \times e^{-E^{0+}_p(t-t_0)}, \tag{18}$$

where m^+ and E^{0+}_p are the nucleon mass and energy, respectively. κ is the hopping parameter in the Wilson fermion action. From now on, we will drop the superscript $+$.

The three-point function for any general operator $\mathcal{O}$ (with color indices suppressed) is defined as

$$G^{\alpha\beta}_{N\mathcal{O}N}(t_2, t_1, \vec{p}_f, \vec{p}_i) = \sum_{\vec{x}_2, \vec{x}_1} e^{-i\vec{p}_f.(\vec{x}_2-\vec{x}_1)}e^{-i\vec{p}_i.(\vec{x}_1-\vec{x}_0)} \times \langle 0|\mathrm{T}(\chi^\alpha(\vec{x}_2, t_2)\mathcal{O}(\vec{x}_1, t_1)\bar{\chi}^\beta(\vec{x}_0, t_0))|0\rangle, \tag{19}$$

where $t = t_2$ is the nucleon sink time, $t = t_1$ is the current insertion time, $t = t_0$ is the nucleon source time, and $\vec{p}_i$ and $\vec{p}_f$ are the initial and final momenta of the nucleon, respectively. For forward matrix element, $\vec{p}_f = \vec{p}_i = \vec{p}$. In this case,

$$G^{\alpha\beta}_{N\mathcal{O}N}(t_2, t_1, \vec{p}) = \sum_{\vec{x}_2, \vec{x}_1} e^{-i\vec{p}.(\vec{x}_2-\vec{x}_0)} \times \langle 0|\mathrm{T}(\chi^\alpha(\vec{x}_2, t_2)\mathcal{O}(\vec{x}_1, t_1)\bar{\chi}^\beta(\vec{x}_0, t_0))|0\rangle. \tag{20}$$

The three-point functions can be classified according to two different topologies of the quark paths [36–39] between the source and the sink of the proton—one is *quark line connected* and the other is *quark line disconnected*.

The *quark line connected* part of the three-point function in the path integral is represented diagrammatically in Fig. 1(a). It needs to be stressed that it is not a Feynman diagram in perturbation theory. We see that the nucleon interpolating quark fields contract with the quark fields of the current so that the quark lines flow continuously from $t = t_0$ at the nucleon source to $t = t_2$ at the nucleon sink. This is termed the *connected insertion* (C.I.). The *quark line disconnected* part is represented diagrammatically in Fig. 1(b). In this case, we see that the quark fields in the current self contract to form a loop, which is disconnected from the nucleon interpolating quark fields with regard to

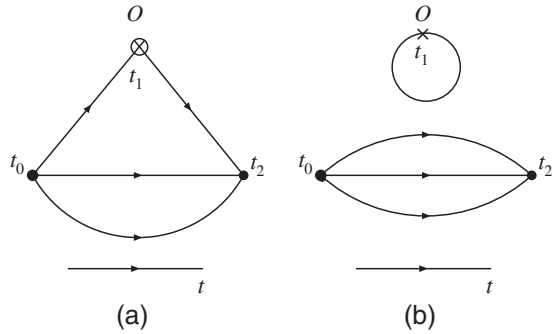

FIG. 1. Quark line diagrams of the three-point function in the Euclidean path-integral formalism. (a) Connected insertion and (b) disconnected insertion.

their quark lines. This is termed the *disconnected insertion* (D.I.). Since the quarks are propagating in the gauge background, if we were to consider a similar situation in terms of Feynman diagrams in the perturbative approach, it would involve gluon lines between the quark loop and the nucleon propagator so that the corresponding Feynman diagrams are *connected* in this sense. Indeed the corresponding disconnected Feynman diagrams are subtracted as the uncorrelated part in the definition of the *disconnected insertion* (D.I.) i.e.

$$G_{N\mathcal{O}N}(\text{D.I.}) = \langle \chi \mathcal{O} \bar{\chi} \rangle - \langle \mathcal{O} \rangle \langle \chi \bar{\chi} \rangle, \tag{21}$$

where χ is the nucleon interpolation field. In the literature, this disconnected insertion is sometimes referred to as the ''disconnected diagram'' which can cause some confusion.

The computation of the C.I. is relatively straight forward. We shall use the sequential source technique [27,40–42] to calculate it. This fixes the source point t_0 and the sink time slice t_2. However, the computation of the D.I. poses a major numerical challenge. The D.I. contains not only the usual propagators from the source, x_0, to any point, x, but also the propagators from any insertion position (x_1) to any other lattice points. This amounts to inverting the fermion matrix at each point of the lattice to construct the *all-to-all* propagators. This entails inversion of a million by million ($\sim 16^3 \times 24 \times 3 \times 4$) sparse matrix on a $16^3 \times 24$ lattice (3 and 4 are number of color and spin indices) for each gauge configuration. This is unattainable even by using the computing powers of today's supercomputers. Instead, we shall calculate with the stochastic method. Specifically, we adopt the complex Z_2 noise for the estimation with unbiased subtraction. The detailed description of the method and the usefulness of discrete symmetries will be presented in Sec. III A.

C. Ratios of correlation functions

In order to extract $\langle x \rangle$ and $\langle x^2 \rangle$, we take the suitable ratios of the three-point to two-point correlation functions. Since, for the case of C.I., the nucleon sink time is fixed, and for the case of D.I., the sink time is not fixed, the procedures for extracting the matrix elements, after taking the ratios, are different for the two cases.

1. Connected insertions

In view of the fact that the matrix elements of $\mathcal{O}_{4i}$, between the equal momentum nucleon states, are proportional to p_i, and that of $\tilde{\mathcal{O}}_{4ii}$ are proportional to p_i^2, and that the momentum projection is folded in the sequential source at the sink time t_2 in the connected insertion calculation, we have chosen only one momentum for the nucleon to be $p_i = 2\pi/La$ (the lowest available nonzero momentum) along the x direction in order to reduce the computational cost.

After inserting complete sets of physical states between the interpolation fields and the operators $\mathcal{O}$, we arrive at the asymptotic relations for the following ratios of three- to two-point functions at $(t_1 - t_0) \gg 1$ and $(t_2 - t_1) \gg 1$:

$$\frac{2\kappa}{p_i} \frac{\text{Tr}[\Gamma G_{N\mathcal{O}_{4i}N}(t_2, t_1, p_i)]}{\text{Tr}[\Gamma G_{NN}(t_2, p_i)]} \xrightarrow{(t_1-t_0)\gg 1,(t_2-t_1)\gg 1} \langle x \rangle. \tag{22}$$

In practice, one takes a plateau in the insertion time, t_1, to define the asymptotic region.

Similarly, we get for the other two operators

$$\frac{2\kappa E_p^0}{(E_p^0)^2 - \frac{1}{3}p_i^2} \frac{\text{Tr}[\Gamma G_{N\tilde{\mathcal{O}}_{44}N}(t_2, t_1, p_i)]}{\text{Tr}[\Gamma G_{NN}(t_2, p_i)]} \xrightarrow{(t_1-t_0)\gg 1,(t_2-t_1)\gg 1} \langle x \rangle, \tag{23}$$

and

$$\frac{2\kappa}{p_i^2} \frac{\text{Tr}[\Gamma G_{N\tilde{\mathcal{O}}_{4ii}N}(t_2, t_1, p_i)]}{\text{Tr}[\Gamma G_{NN}(t_2, p_i)]} \xrightarrow{(t_1-t_0)\gg 1,(t_2-t_1)\gg 1} \langle x^2 \rangle. \tag{24}$$

2. Disconnected insertions

As seen from Fig. 1(b), the calculation of the valence quark propagators in the disconnected insertion is separate from the loop calculation in each configuration; this means that the momentum in the three-point function can be chosen in the nucleon two-point functions independent of the expensive loop calculation. For the present calculation, we choose $p_i = \pm 2\pi/La$ for the three-point function for the cases of $\mathcal{O}_{4i}$ and $\tilde{\mathcal{O}}_{4ii}$, and zero momentum for $\tilde{\mathcal{O}}_{44}$.

In contrast to C.I., the sink time need not be fixed in D.I. We can sum over the insertion time to gain more statistics [43–46]. There are various methods by which the summation is performed [46–49]. All these methods, except in [46], considered summation over insertion time up to or beyond sink time. From Appendix A, we see that the matrix elements for the twist-two operators are analytically zero if $t_1 < t_0$ and $t_1 > t_2$. (It may not be zero for other operators. Even then it will not contribute to the physical quantity intended to be measured). So the summation outside the nucleon source and sink times will contribute to unnecessary noise and possible contribution from higher

states which are unrelated to the target matrix element. Also, at the source and sink time it can have contributions from the contact term. In view of the above, we shall take the sum to be from (source time $+1$) to (sink time -1) [46]. According to the derivations in Appendix A 2 (see Eq. (A10)), under the condition $t_2 - t_0 \gg 1$, we get for the operator $\mathcal{O}_{4i}$

$$\sum_{t_1=t_0+1}^{t_2-1} \frac{2\kappa}{p_i} \frac{\mathrm{Tr}[G_{N\mathcal{O}_{4i}N}(t_2, t_1, p_i)]}{\mathrm{Tr}[\Gamma G_{NN}(t_2, p_i)]} \xrightarrow{(t_2-t_0)\gg 1} \langle x\rangle_{4i} t_2 + \text{const} \tag{25}$$

Similarly, for the other two operators, we get

$$\sum_{t_1=t_0+1}^{t_2-1} \frac{2\kappa}{E_p^0} \frac{\mathrm{Tr}[G_{N\tilde{\mathcal{O}}_{44}N}(t_2, t_1, 0)]}{\mathrm{Tr}[\Gamma G_{NN}(t_2, 0)]} \xrightarrow{(t_2-t_0)\gg 1} \langle x\rangle_{44} t_2 + \text{const}, \tag{26}$$

and

$$\sum_{t_1=t_0+1}^{t_2-1} \frac{2\kappa}{p_i^2} \frac{\mathrm{Tr}[G_{N\tilde{\mathcal{O}}_{4ii}N}(t_2, t_1, p_i)]}{\mathrm{Tr}[\Gamma G_{NN}(t_2, p_i)]} \xrightarrow{(t_2-t_0)\gg 1} \langle x^2\rangle_{4ii} t_2 + \text{const}. \tag{27}$$

III. DISCONNECTED INSERTION CALCULATION

The D.I. calculation is the most numerically intensive part. We shall discuss the various aspects of the calculation in more detail.

A. Discrete symmetries and transformations

Since the D.I. calculations are performed by using a stochastic noise estimator, the signals for the current loop are always noisy. We can reduce the errors by making good use of some of the discrete symmetries, specifically parity, γ_5 Hermiticity, and charge-γ_5 Hermiticity (CH transformation) [47,50–52].

By applying these symmetries and transformations, one can then work out the effects of gauge averaging in order to find out the correct part (e.g. even or odd parity, real or imaginary part, etc.) of the two-point and three-point correlation functions, current operators etc., and discard the irrelevant part.

1. Two-point functions

Since in the case of D.I. the three-point functions are constructed by multiplying the nucleon propagator with the current loop in each gauge configuration [Fig. 1(b)], we have the advantage of taking into account nucleon propagators with equal and opposite momenta in order to increase statistics. While doing so, we have to consider the fact that such combinations have appropriate parity and have appropriate real or imaginary part w.r.t. the loop. In Table I, we show the effect of parity and CH transformations on various such combinations. We denote $\mathrm{Tr}[\Gamma G_{NN}(t, \vec{p}; U)]$ to be the nucleon propagator on each gauge configuration with momentum $\vec{p}$.

2. Current loop

The outcome of the parity, γ_5 Hermiticity, and CH transformations for the operators $\mathcal{O}_{4i}$, $\tilde{\mathcal{O}}_{44}$, and $\tilde{\mathcal{O}}_{4ii}$ on each gauge configuration are shown in Table II. The notation "Im" includes the factor i of the imaginary part of each operator.

3. Correlations between the nucleon propagator and the loop

When determining the correlation between the appropriate parts of the nucleon propagator and the loop, we

TABLE I. Table showing the outcome of the CH and parity transformations on the combinations of nucleon propagators with equal and opposite momenta. U^p is the parity transformed gauge link.

Nucleon Propagators	*CH Transformations*	*Parity*
$\mathrm{Tr}[\Gamma G_{NN}(t, \vec{p}; U)]$	$\mathrm{Tr}[\Gamma G_{NN}(t, -\vec{p}; U^*)]^*$	$\mathrm{Tr}[\Gamma G_{NN}(t, -\vec{p}; U^p)]$
$\mathrm{Tr}[\Gamma G_{NN}(t, \vec{p}; U)]$ $-\mathrm{Tr}[\Gamma G_{NN}(t, -\vec{p}; U)]$	$-\{\mathrm{Tr}[\Gamma G_{NN}(t, \vec{p}; U^*)]$ $-\mathrm{Tr}[\Gamma G_{NN}(t, -\vec{p}; U^*)]\}^*$	Odd
$\mathrm{Tr}[\Gamma G_{NN}(t, \vec{p}; U)]$ $+\mathrm{Tr}[\Gamma G_{NN}(t, -\vec{p}; U)]$	$\{\mathrm{Tr}[\Gamma G_{NN}(t, \vec{p}; U^*)]$ $+\mathrm{Tr}[\Gamma G_{NN}(t, -\vec{p}; U^*)]\}^*$	Even

TABLE II. Table showing the outcome of the parity transformations, γ_5 Hermiticity and CH Transformations on current loops. L stands for current loop and Im includes the factor i of the imaginary part.

Loops	*Parity*	*γ_5 Hermiticity*	*CH Transformations*	*γ_5 Hermiticity & CH Transformations Combined*
$\mathcal{O}_{4i}$	Odd	Imaginary	$[\mathrm{L}]_U = -[\mathrm{L}_{U^*}]^*$	$\mathrm{Im}[\mathrm{L}]_U = \mathrm{Im}[\mathrm{L}]_{U^*}$
$\mathcal{O}_{44} - \frac{1}{3}(\mathcal{O}_{11} + \mathcal{O}_{22} + \mathcal{O}_{33})$	Even	Real	$[\mathrm{L}]_U = [\mathrm{L}_{U^*}]^*$	$\mathrm{Re}[\mathrm{L}]_U = \mathrm{Re}[\mathrm{L}]_{U^*}$
$\mathcal{O}_{4ii} - \frac{1}{2}(\mathcal{O}_{4jj} + \mathcal{O}_{4kk})$	Even	Imaginary	$[\mathrm{L}]_U = [\mathrm{L}_{U^*}]^*$	$\mathrm{Im}[\mathrm{L}]_U = -\mathrm{Im}[\mathrm{L}]_{U^*}$

TABLE III. The relevant parts considered for D.I. calculations for the nucleon propagator and the corresponding loops based on parity, γ_5 Hermiticity, and CH theorem.

Nucleon Propagators	*Loops*
$\mathrm{Im}[\mathrm{Tr}[\Gamma G_{NN}(t,\vec{p};U)]-\mathrm{Tr}[\Gamma G_{NN}(t,-\vec{p};U)]]$	$\mathrm{Im}[\mathcal{O}_{4i}]$
$\mathrm{Re}[\mathrm{Tr}[\Gamma G_{NN}(t,0;U)]]$	$\mathrm{Re}[\mathcal{O}_{44}-\frac{1}{3}(\mathcal{O}_{11}+\mathcal{O}_{22}+\mathcal{O}_{33})]$
$\mathrm{Im}[\frac{1}{2}[\mathrm{Tr}[\Gamma G_{NN}(t,p_i;U)]+\mathrm{Tr}[\Gamma G_{NN}(t,-p_i;U)]]]$	$\mathrm{Im}[\mathcal{O}_{4ii}-\frac{1}{2}(\mathcal{O}_{4jj}+\mathcal{O}_{4kk})]$

have to consider the three-point function as a whole. As an example, if we consider two-point functions with both the momenta $\pm p_i$ for the operator $\mathcal{O}_{4i}$, then from Eq. (25), we get

$$\sum_{t_1=t_0+1}^{t_2-1}\frac{\kappa}{p_i}\frac{\mathrm{Tr}[G_{N\mathcal{O}_{4i}N}(t_2,t_1,p_i)]-\mathrm{Tr}[G_{N\mathcal{O}_{4i}N}(t_2,t_1,-p_i)]}{\mathrm{Tr}[\Gamma G_{NN}(t_2,p_i)]} = \langle x\rangle t_2 + \text{const.} \tag{28}$$

So, for $\mathcal{O}_{4i}$ which is odd in parity, one can explicitly consider the odd combination of the nucleon propagators in Table I, and similarly, the even combinations for $\tilde{\mathcal{O}}_{44}$ and $\tilde{\mathcal{O}}_{4ii}$, to reduce noise. According to the *CH* theorem [47,50,51], the path integral for $\langle\mathcal{O}\rangle$ in QCD is either real or imaginary (except in the case with chemical potential). It can be shown from Tables I and II that if we combine the *CH* transformation of the nucleon propagators (with the appropriate combination or parity) and the loop, the three-point functions transform to the positive complex conjugate of themselves on the link U for all the 3 D.I. cases considered here. This, according to the *CH* theorem, means that the three-point functions are real. Since, by using γ_5 Hermiticity we see that the loops are either real or imaginary (Table II); one needs to multiply them with only the real or imaginary part of the nucleon propagators to make the three-point functions real. For example, the left-hand side of Eq. (28) can be written as

$$\begin{aligned}
&\frac{1}{2}[\mathrm{Tr}[G_{N\mathcal{O}_{4i}N}(t_2,t_1,p_i)]-\mathrm{Tr}[G_{N\mathcal{O}_{4i}N}(t_2,t_1,-p_i)]]\\
&=\frac{1}{2N_g}\sum_j\Big[\frac{1}{2}[\mathrm{Tr}[\Gamma G_{NN}(t,p_i;U^j)]-\mathrm{Tr}[\Gamma G_{NN}(t,-p_i;U^j)]]\times\mathrm{Im}(\mathrm{Loop})_{U^j},\\
&\quad+\frac{1}{2}[\mathrm{Tr}[\Gamma G_{NN}(t,p_i;U^{*j})]-\mathrm{Tr}[\Gamma G_{NN}(t,-p_i;U^{*j})]]\times\mathrm{Im}(\mathrm{Loop})_{U^{*j}}\Big]\\
&=\frac{1}{2N_g}\sum_j\mathrm{Im}\{\mathrm{Tr}[\Gamma G_{NN}(t,p_i;U^j)]-\mathrm{Tr}[\Gamma G_{NN}(t,-p_i;U^j)]\}\times\mathrm{Im}(\mathrm{Loop})_{U^j},
\end{aligned}\tag{29}$$

where N_g is the number of gauge configurations. As illustrated above, one can exclude the real part of the nucleon propagator and the real part of the loop for $\mathcal{O}_{4i}$ operator which contributes to noise with finite number of noise vectors. The utilization of γ_5 Hermiticity and *CH* theorem has been shown to reduce noise effectively in the loop calculation of the quark angular momentum [47]. Similar procedures can be applied to the other two operators. We show in Table III the relevant parts of the nucleon propagator(s) and the corresponding loop in each row which are to be correlated on each gauge configuration.

B. Complex Z_2 noise and unbiased subtraction method

As we mentioned in Sec. II B, it is a numerical challenge to evaluate the quark loop. We shall adopt the complex Z_2 noise with unbiased subtraction to calculate it.

The basic idea of the complex Z_2 noise method [53] is to construct L noise vectors, $\eta^1,\eta^2\ldots\ldots\eta^L$ (each of dimension $N\times 1$), where $\eta^j=\{\eta_1^j,\eta_2^j,\ldots\eta_N^j\}$, in order to stochastically estimate the inversion of an $N\times N$ matrix. Each element η_n^j takes one of the four values, $\frac{1}{\sqrt{2}}\{\pm 1\pm i\}$, chosen independently with equal probability. They have the properties of a white noise

$$\begin{aligned}
\langle\eta_i\rangle&=\lim_{L\to\infty}\frac{1}{L}\sum_{n=1}^{L}\eta_i^n=0,\\
\langle\eta_i^\dagger\eta_j\rangle&=\lim_{L\to\infty}\frac{1}{L}\sum_{n=1}^{L}\eta_i^{\dagger n}\eta_j^n=\delta_{ij},\qquad \eta_i^\dagger\eta_i=1.
\end{aligned}\tag{30}$$

Then, the expectation value of the matrix element M_{ij}^{-1} is obtained by solving for X_i in the matrix equations $MX=\eta$, so that

$$E[M_{ij}^{-1}]=\langle\eta_j^\dagger X_i\rangle=\sum_k M_{ik}^{-1}\langle\eta_i^\dagger\eta_k\rangle=M_{ij}^{-1}. \tag{31}$$

It has been shown [53–55] that the variance corresponding to the estimator is given by

$$\sigma_M^2 = \frac{1}{L}\sum_{m\neq n}^{N} |M^{-1}_{m,n}|^2, \tag{32}$$

which is minimal, since it does not involve the positive contribution from the diagonal matrix elements as do in other type of noises, such as the Gaussian noise. It is in this sense, Z_2 noise is considered optimal [53–55]. Similarly, one can show that $Z(N)$ and $U(1)$ noises are also optimal.

It has been further shown that the off-diagonal matrix element contributions to the variance in Eq. (32) can be reduced by subtracting a judiciously chosen set of traceless $N \times N$ matrices $Q^{(p)}$ [47,52,55], which satisfy $\sum_{n=1}^{N} Q^{(p)}_{n,n} = 0$, $p = 1, \cdots, P$. Then the expectation value is unchanged when M^{-1} is substituted with $M^{-1} - \sum_{p=1}^{P} \lambda_p Q^{(p)}$ (λ_p is a constant)

$$E[\langle \eta^\dagger (M^{-1} - \sum_{p=1}^{P} \lambda_p Q^{(p)})\eta\rangle] = \mathrm{Tr} M^{-1}, \tag{33}$$

while the variance becomes

$$\sigma_M^2 = \mathrm{Var}\left[\left\langle \eta^\dagger \left(M^{-1} - \sum_{p=1}^{P} \lambda_p Q^{(p)}\right)\eta\right\rangle\right] = \frac{1}{L}\sum_{m\neq n}^{N}\left| M^{-1}_{m,n} - \sum_{p=1}^{P}\lambda_p Q^{(p)}_{m,n}\right|^2. \tag{34}$$

So, with a judicious choice of traceless matrix, the variance may be reduced when the off-diagonal matrix elements of $Q^{(p)}$ are correlated with those of M^{-1}. This subtraction is unbiased, because it does not change the expectation value of the trace. The natural choice for the set of traceless matrices is the hopping parameter expansion of the inverse of the Wilson fermion matrix, M [55], given by

$$M^{-1} = I + \kappa D + \kappa^2 D^2 + \kappa^3 D^3 + \cdots, \tag{35}$$

where

$$D_{x,y} = \sum_{\mu=1}^{4}[(1-\gamma_\mu)_{\alpha\beta} U^{ab}_\mu(x)\delta_{x,y-a_\mu} + (1+\gamma_\mu)_{\alpha\beta} U^{\dagger ab}_\mu(x-a_\mu)\delta_{x,y+a_\mu}], \tag{36}$$

which is off-diagonal in space-time.

In evaluating the quark loop, we shall consider the following subtraction

$$\langle \eta^\dagger Q'[M^{-1} - (I + \kappa D + \kappa^2 D^2 + \kappa^3 D^3 + \ldots)]\eta\rangle + \text{traces}, \tag{37}$$

where Q' represent operators between the fermion fields in $\mathcal{O}_{4i}$, $\tilde{\mathcal{O}}_{44}$, and $\tilde{\mathcal{O}}_{4ii}$. Traces may arise while combining the operators Q' with the hopping expansion in Eq. (35), leading to nonzero traces at certain power(s) of D. In this case, one needs to evaluate these traces and add them back to cancel out those which are subtracted out in the noise estimation. The details of the trace calculations for these operators are given in Appendix B. Since the calculations of traces are cumbersome for large loops, we will restrict ourselves only up to $\kappa^4 D^4$ for two-index operators and $\kappa^3 D^3$ for three-index operators. We shall now discuss these trace terms here.

1. Traces for two-index operators $\mathcal{O}_{4i}$ and $\mathcal{O}_{\mu\mu}$

Since Q' for $\mathcal{O}_{4i}$ and $\mathcal{O}_{\mu\mu}$ are point-split, the traces for the first subtraction terms, i.e. $\mathrm{Tr}(Q'I)$, are zero. So we can use it for subtraction. However, from Appendix B, we see that the noise estimate is real for $\mathcal{O}_{4i}$ while the exact loop $\mathrm{Tr}(Q'M^{-1})$ is imaginary (see Sec. III A). Similarly, the noise estimate is imaginary for $\mathcal{O}_{\mu\mu}$ while the exact loop $\mathrm{Tr}(Q'M^{-1})$ is real. Therefore, there is no use to include this subtraction term. The subtraction with $\kappa^2 D^2$ and $\kappa^4 D^4$ terms in the hopping expansion are also traceless, since the multiplication of Q' to these terms does not lead to a plaquette which is the lowest order in κ that contributes to a trace. On the other hand, the κD and $\kappa^3 D^3$ terms can lead to a plaquette, thus can have nonzero traces. Since the operators, $\mathcal{O}_{4i}$ and $\mathcal{O}_{\mu\mu}$, lead to different traces, we shall consider them separately.

In the case of $\mathcal{O}_{4i}$, the contribution from the hopping expansion terms κD, $\kappa^2 D^2$, $\kappa^3 D^3$ and $\kappa^4 D^4$ are traceless (Appendix B). One does not have to worry about the complication of having to add back the trace contributions.

But, $\mathcal{O}_{\mu\mu}$ operator has nonzero traces when combined with κD and $\kappa^3 D^3$ (see Appendix B for a full derivation). The trace for the κD term is $\frac{\lambda}{8a} 96 \kappa V_3$, where V_3 is the three-volume of the lattice used, and $\lambda = +1$ for $\mu = \nu = 1, 2, 3$, and $\lambda = -1$ for $\mu = \nu = 4$. And, for $\kappa^3 D^3$ [see Fig. 2(a)], it is

$$\frac{\lambda}{8a} 32\kappa^3 \sum_{\vec{x}_1}\sum_{m}\sum_{\mu'\neq\mu} \mathrm{Re}[\{U_{\mu'}(x_1+a_\mu)U^\dagger_\mu(x_1+a_{\mu'})U^\dagger_{\mu'}(x_1)U_\mu(x_1) + U_\mu(x_1)U^\dagger_{\mu'}(x_1+a_\mu-a_{\mu'})U^\dagger_\mu(x_1-a_{\mu'}) \times U_{\mu'}(x_1-a_{\mu'}) + U_\mu(x_1-a_\mu+a_{\mu'})U^\dagger_{\mu'}(x_1)U^\dagger_\mu(x_1-a_\mu)U_{\mu'}(x_1-a_\mu) + U_{\mu'}(x_1-a_{\mu'})U^\dagger_\mu(x_1-a_\mu) \times U^\dagger_{\mu'}(x_1-a_\mu-a_{\mu'})U_\mu(x_1-a_\mu-a_{\mu'})\}^{mm}]. \tag{38}$$

These traces need to be added as shown in Eq. (37).

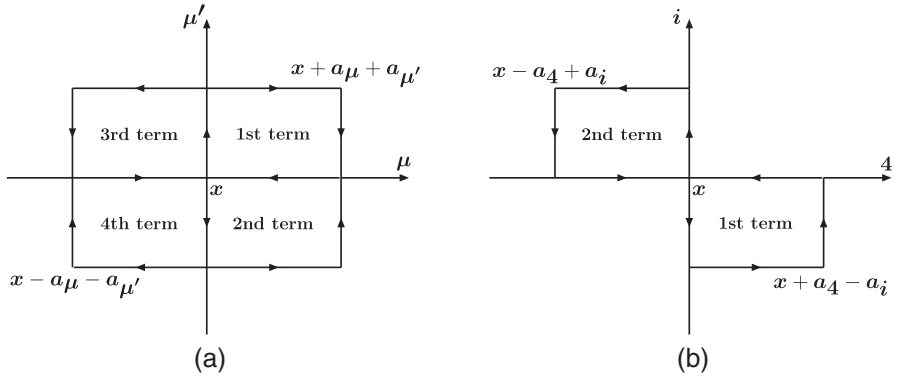

FIG. 2. Plaquette terms (a) for the operator $\mathcal{O}_{\mu\mu}$ when $\kappa^3 D^3$ term is considered and (b) for $\mathcal{O}_{4ii}$ when $\kappa^2 D^2$ term is considered.

2. Traces for three-index operators

For the three-index operator, the noise estimator is real for the first term, I. But from γ_5 Hermiticity we see that the loop for $\tilde{\mathcal{O}}_{4ii}$ is imaginary. Thus, it is not useful to consider this term in subtraction. Up to $\kappa^3 D^3$, the only trace contribution comes from the $\kappa^2 D^2$ term, which is (see Appendix B for a full derivation)

$$\frac{1}{24a^2} 16\kappa^2 \sum_{\vec{x}_1} \Bigg[\sum_m \mathrm{Im}\{U_4^\dagger(x_1 - a_i) U_i(x_1 - a_i) U_4(x_1) \times U_i^\dagger(x_1 + a_4 - a_i)\}^{mm} + \sum_m \mathrm{Im}\{U_4(x_1 - a_4 + a_i) U_i^\dagger(x_1) U_4^\dagger(x_1 - a_4) \times U_i(x_1 - a_4)\}^{mm} \Bigg]. \tag{39}$$

The graphical representation for this trace is illustrated in Fig. 2(b).

3. Numerical test

It is necessary to check that the analytical calculations for trace for each subtraction term is correct. In order to do that we have to calculate the subtraction terms exactly. We did it on a smaller (4^4) lattice as described below.

From the matrix equation $MX = \eta$, we have

$$X\eta^\dagger = M^{-1}\eta\eta^\dagger = (I + \kappa D + \kappa^2 D^2 + \kappa^3 D^3 + \kappa^4 D^4 + \cdots)\eta\eta^\dagger. \tag{40}$$

From Eq. (40) we see that we can exactly calculate M^{-1} *i.e.* each subtraction term, only if $\eta\eta^\dagger$ is a unit matrix. By choosing the following orthogonal set of vectors $\{\eta_i\}$

$$\{\eta_i\} = \left\{ \begin{pmatrix} 1 \\ 0 \\ 0 \\ \vdots \\ \vdots \end{pmatrix}, \begin{pmatrix} 0 \\ 1 \\ 0 \\ \vdots \\ \vdots \end{pmatrix}, \begin{pmatrix} 0 \\ 0 \\ 1 \\ \vdots \\ \vdots \end{pmatrix}, \ldots, \begin{pmatrix} \vdots \\ \vdots \\ \vdots \\ 0 \\ 0 \\ 1 \end{pmatrix} \right\}, \tag{41}$$

we obtain $\eta\eta^\dagger = \frac{1}{L}\sum_i^L \eta_i \eta_i^\dagger = \mathbb{1}$. Using these vectors, we compute I, κD, $\kappa^2 D^2$, $\cdots$ for each operator. We have found that our numerical results matched with those of analytical expressions e.g. for $\mathcal{O}_{4i}$ operator, the terms κD, $\kappa^2 D^2$, $\kappa^3 D^3$, and $\kappa^4 D^4$ terms have no traces.

IV. RENORMALIZATION

The physical matrix elements, which are determined from a linear extrapolation to the chiral limit, are extracted in lattice units from the Monte Carlo calculation. In order to relate to the experimental values, they have to be expressed in physical units and renormalized at a certain scale. The renormalized operators, at a finite energy scale μ, are related to the bare lattice operators through the renormalization constant

$$\mathcal{O}(\mu) = Z_{\mathcal{O}}(a\mu, g(a))\mathcal{O}(a), \tag{42}$$

where g is the bare coupling constant, which is equal to one in our case. The renormalization constants, Z's, are computed by using perturbation theory. We will use the values of Z factors, which are computed in [56] by using tadpole-improved perturbation theory [57]. Since the experimental results are often renormalized in the $\overline{\mathrm{MS}}$ scheme, we will also use the calculated Z factors matched to this scheme. In the quenched approximation, the renormalization constants are

$$Z_{\mathcal{O}}(a\mu, g^*) = \frac{u_0}{u_0^{n_D}} \Bigg(1 - \frac{g^{*2}}{16\pi^2} C_F \Bigg(\gamma_{\mathcal{O}} \ln(a\mu) + B_{\mathcal{O}}^{\overline{\mathrm{MS}}} + (n_D - 1) 8\pi^2 Z_0\Bigg) + O(g^{*4})\Bigg), \tag{43}$$

TABLE IV. The values of $\gamma_{\mathcal{O}}$ and $B_{\mathcal{O}}^{\overline{\rm MS}}$ for all the three operators under consideration.

Operators	$\gamma_{\mathcal{O}}$	$B_{\mathcal{O}}^{\overline{\rm MS}}$
$\mathcal{O}_{4i}$	$\frac{16}{3}$	1.279
$\tilde{\mathcal{O}}_{44}$	$\frac{16}{3}$	2.561
$\tilde{\mathcal{O}}_{4ii}$	$\frac{25}{3}$	−12.128

where

$$u_0 = \left\langle \frac{1}{3}\,\mathrm{Tr}U_{\rm plaq}\right\rangle^{1/4}, \qquad g^{*2} = \frac{g^2}{u_0^4}, \qquad C_F = \frac{4}{3}, \qquad Z_0 = 0.155, \tag{44}$$

and $\gamma_{\mathcal{O}}$ is the anomalous dimension of the operator, $\bar{B}_{\mathcal{O}}$ is the finite part of $Z_{\mathcal{O}}$, and n_D is the number of covariant derivative(s) in the operator. We list the values $\gamma_{\mathcal{O}}$ and $\bar{B}_{\mathcal{O}}^{\overline{MS}}$ in Table IV for the three operators we consider.

Our inverse lattice spacing is determined to be $1/a = 1.74$ GeV [47] by using nucleon mass. The value of $u_0 = \langle \frac{1}{3}\,\mathrm{Tr}U_{\rm plaq}\rangle^{1/4} = 0.88$ is obtained from Ref. [58]. By using all the relevant factors for a particular operator, we get the renormalization factors at $\mu = 2$ GeV ($\mu^2 = 4$ GeV^2) scale for the following operators as

$$\mathcal{O}_{4i}\colon Z_{\mathcal{O}_{4i}} = 0.972, \qquad \tilde{\mathcal{O}}_{44}\colon Z_{\mathcal{O}_{44}} = 0.953, \qquad \tilde{\mathcal{O}}_{4ii}\colon Z_{\mathcal{O}_{4ii}} = 1.116. \tag{45}$$

Also, in the tadpole-improved mean-field approach, there is a finite ma correction factor f for the Wilson fermion in the case of fermion bilinear operators [44,58,59]

$$f = \frac{e^{m_q a}}{8\kappa_c}\,\frac{1}{\langle \frac{1}{3}\,\mathrm{Tr}U_{\rm plaq}\rangle^{1/4}}, \qquad m_q a = \ln\!\left(\frac{4\kappa_c}{\kappa} - 3\right), \tag{46}$$

with the critical $\kappa_c = 0.1568$ [58]. The values of f for $\kappa = 0.154$, 0.155, and 0.1555 (which are used for our calculations) are 0.972, 0.948, and 0.936, respectively.

V. NUMERICAL PARAMETERS AND ERROR STUDIES

We use 500 gauge configurations on a $16^3 \times 24$ lattice generated with Wilson action at $\beta = 6.0$ in the quenched approximation. They are produced by the pseudoheatbath algorithm with 10 000 sweeps between consecutive configurations. The values of the hopping parameter we have used are $\kappa = 0.154$, 0.155 and 0.1555. For the disconnected insertion, we shall define two κ's for the quark masses: κ_v for valence quarks, and $\kappa_{\rm sea}$ for sea quarks. For the strange quark currents we have fixed $\kappa_{\rm sea} = 0.154$, which is close to the strange quark mass as determined from the ϕ meson mass and k_v takes the values of 0.154, 0.155, and 0.1555. The critical hopping parameter, $\kappa_c = 0.1568$ is obtained by a linear extrapolation to the zero pion mass [58]. Using the nucleon mass to set the lattice spacing at $a = 0.11$ fm, the corresponding pion masses are 650(3), 538(4), and 478(4) MeV, and the nucleon masses are 1291(9), 1159(11), and 1093(13) MeV, respectively. We have used Dirichlet boundary condition in the present work. We should note that there is a large uncertainty in determining the lattice spacing in the quenched approximation, as much as ∼20%. For example, using $r_0 = 0.5$ fm to set the scale, the lattice spacing would be $a = 0.09$ fm. Thus, using this scale, the dimensionful quantities will be shifted by ∼20%. Since we are calculating the moments $\langle x\rangle$ and $\langle x^2\rangle$ which are dimensionless, the results we report here will not depend on the scale of the lattice spacing except for the renormalization constant which has an negligible difference between these two lattice spacings.

(i) For the connected insertion, we have chosen the number of independently generated gauge configurations to be 200, and for disconnected insertion it is 500. The maximum number of noise, used for DI, is 400 for each gauge configuration.

(ii) The error analysis has been performed by using the jackknife procedure [60,61]. Since the computations for all the time slices and quark masses has been performed using the same set of gauge configurations, the data we obtain are correlated in Euclidean time. The correlation among different quantities are taken into account by constructing the corresponding covariance matrices [62–64]. The error bars are obtained by using this method. In order to extract various physical quantities, we have used correlated least-χ^2 fits.

A. Error studies in DI

Since noise estimate plays an essential role for the case of the disconnected insertion, we shall study the effect of number of noise and gauge configurations on the error for the signal we are extracting. We will present a few results of such studies before discussing the results for the moments of the quark distribution.

The standard error due to the Z_2 noise estimation of the loop averaged over the gauge configurations is given by [65–67]

$$\sigma = \sqrt{\frac{\sigma_g^2}{N_g} + \frac{\sigma_n^2}{N_n N_g}}. \tag{47}$$

where σ_g^2 is the variance of the ensemble of gauge configurations, σ_n^2 is the variance coming from the noise estimator, and N_g and N_n are number of gauge configurations and noise estimator, respectively.

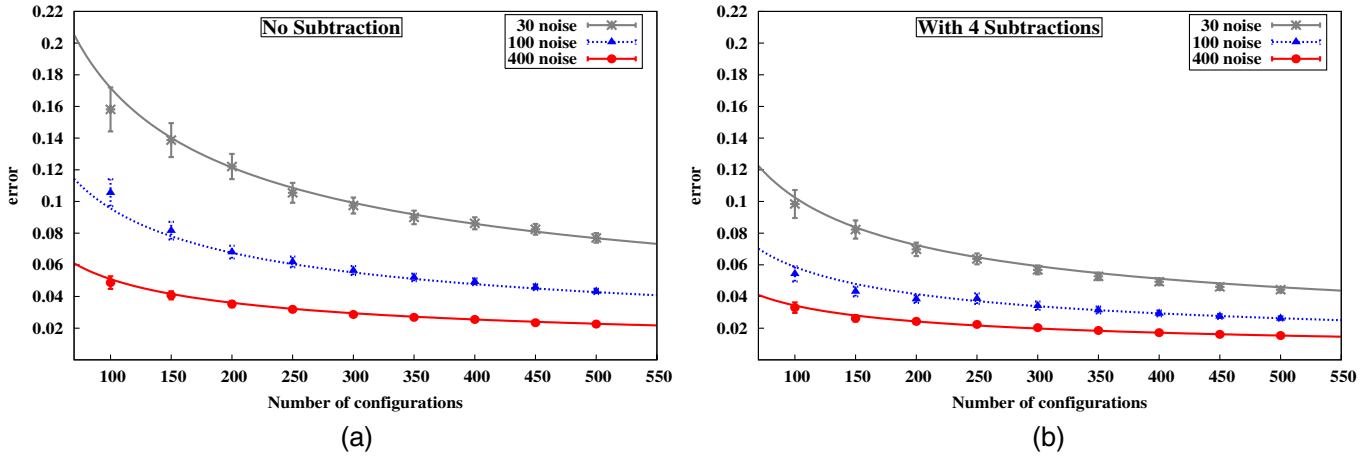

FIG. 3 (color online). Errors of the noise estimation plotted against the number of configurations for different sets of noise vectors for the loop part of the current, $\mathcal{O}_{4i}$ at $\kappa_v = \kappa_{\text{sea}} = 0.154$ and insertion time, $t_1 = 14$ (a) without subtraction and (b) with four subtraction terms.

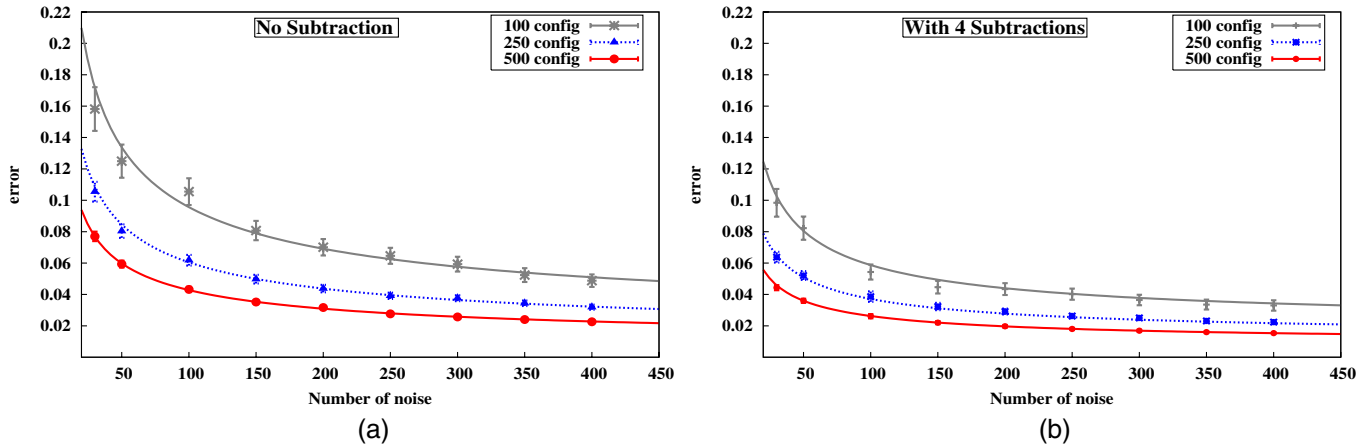

FIG. 4 (color online). Errors of the noise estimation plotted against the number of noise vectors for different sets of configurations for the loop part of the current $\mathcal{O}_{4i}$ at $\kappa_v = \kappa_{\text{sea}} = 0.154$ and insertion time, $t_1 = 14$ (a) without subtraction and (b) with four subtraction terms.

To make sure that our results are generated correctly, we verify that their errors are in conformity with Eq. (47) and extract the standard deviations σ_g and σ_n from the existing data with and without unbiased subtractions.

In Figs. 3(a) and 3(b), we plot the errors of the noise estimation for the loop part of the current $\mathcal{O}_{4i}$ in Eq. (47) at the time slice 14 against the number of gauge configurations for 30, 100 and 400 noise without unbiased subtraction and with four subtraction terms (κD, $\kappa^2 D^2$, $\kappa^3 D^3$ and $\kappa^4 D^4$), respectively. The errors on the errors are obtained by using the double jackknife method on the data. After fitting for σ_g^2 and σ_n^2 from Eq. (47), we see that all the curves can be well described by Eq. (47). Similarly, we plot the errors against the number of noises for 100, 250 and 500 gauge configurations without subtraction and with four subtraction terms in Figs. 4(a) and 4(b) respectively. Again, we see that the curves fit Eq. (47) well. A similar conclusion can be drawn for the other two operators. The central values of the standard deviations, σ_g and σ_n along with their errors are given in Table V for the cases with and without subtractions. These values show that the standard deviations for the gauge configuration and noise ensemble are not of the same order. The standard deviation for noise

TABLE V. Table for the values of standard deviations of gauge configurations and noise for the current $\mathcal{O}_{4i}$ without subtraction and with four subtraction terms.

	σ_{gauge}	σ_{noise}
No Subtraction	0.204 ± 0.063	9.341 ± 0.301
With 4 Subtractions	0.205 ± 0.028	5.500 ± 0.201

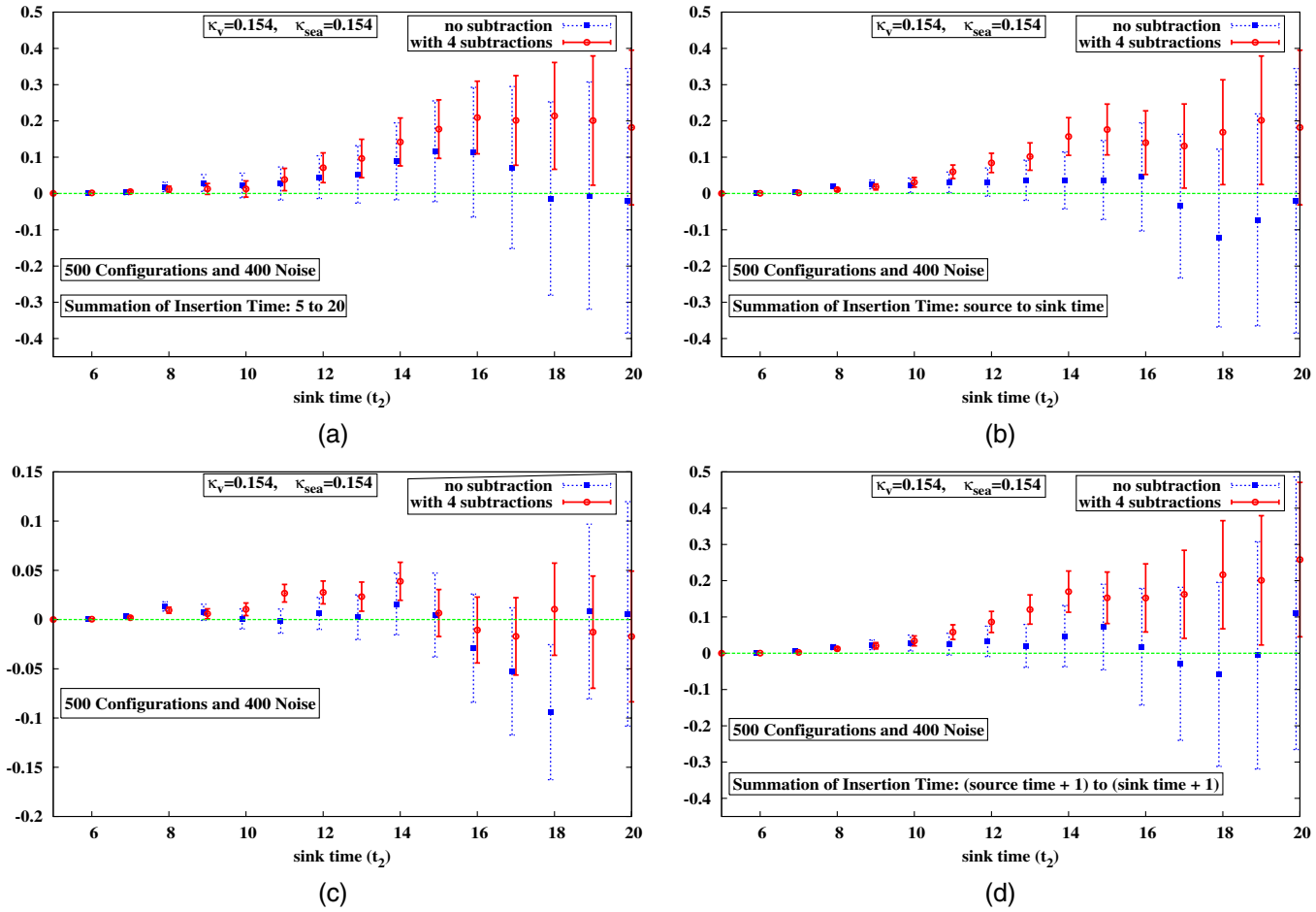

FIG. 5 (color online). The ratio (D.I.) of the three-point to two-point functions at $\kappa_v = \kappa_{\text{sea}} = 0.154$ for the $\mathcal{O}_{4i}$ operator is plotted against the nucleon sink time (t_2) by using four different methods: (a) summation of insertion time from 5 to 20, (b) summation of insertion time from source to sink time, (c) method used in R. Lewis *et al.* [49], and (d) summation of insertion time from (source time $+1$) to (sink time $+1$).

are, in fact, much higher than that for the gauge configuration. Another point to note is that the standard deviation σ_n for the noise is reduced by almost a half with 4-term unbiased subtraction whereas σ_g remains the same.

B. Analysis for DI

As mentioned in Sec. II C 2, we have studied five different methods of summation over insertion time by using the operator $\mathcal{O}_{4i}$ at $\kappa_v = \kappa_{\text{sea}} = 0.154$ shown in Fig. 5. In the first method [48], we have performed the summation of the current insertion starting and ending 4 time slices away from each of the boundary. In our case, it would be from 5 to 20 [Fig. 5(a)]. In the second method [47], the summation has been performed from the source to the sink time of the nucleon propagator [Fig. 5(b)]. The third method is described in [49] [Fig. 5(c)]. The fourth method is an additional study where the summation has been performed from (source time $+1$) to (sink time $+1$) of the nucleon propagator [Fig. 5(d)]. The fifth method used in [46] and described in Sec. II C 2 [Fig. 6(a)]. In this method, the summation has been performed from (source time $+1$) to (sink time -1) of the nucleon propagator. In the first, second, fourth, and fifth methods, the slopes (given by Eq. (25)) are fitted between the time slices 10 and 14 in order to extract the signal. And in the third method, a constant is fitted between 11 and 14. The values are provided in Table VI. We see that the all these methods are consistent with each other. For our present work, we adopt the fifth method.

C. Multiple sources for DI

In the case of D.I., we have the liberty of choosing quark propagators at different source locations on the lattice with much less overhead that the C.I. computation which involves generating additional quark propagators using the sequential source method. We correlate these nucleon propagators at different source locations with the already computed loop to increase statistics. We have used 1, 4, and 16 different sources. This results in significant reduction of error bars which is presented in Sec. VI.

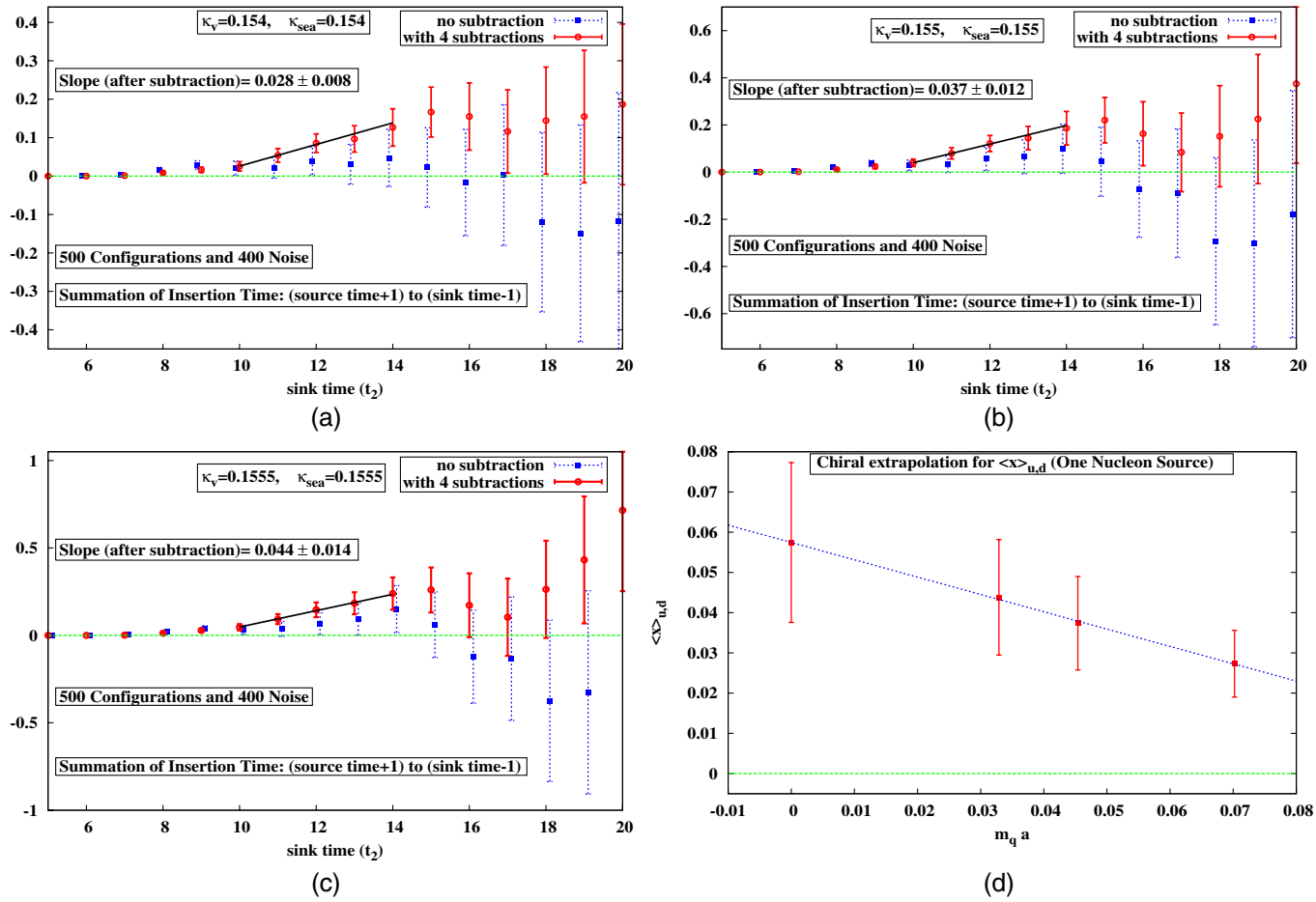

FIG. 6 (color online). The ratio of the three-point to two-point functions (summed over insertion time) for the $\mathcal{O}_{4i}$ operator, for the case with equal valence and sea quark masses, is plotted against the nucleon sink time (t_2) at (a) $\kappa_v = \kappa_{\text{sea}} = 0.154$, (b) $\kappa_v = \kappa_{\text{sea}} = 0.155$, and (c) $\kappa_v = \kappa_{\text{sea}} = 0.1555$. (d) is a linear extrapolation to the chiral limit for the first moment, $\langle x \rangle_{u,d}$, (D.I.) of the up (down) quark which is plotted against $m_q a$.

VI. RESULTS

In this section, we will present results for the first and second moments of nucleon's parton distribution function for both the disconnected insertion and the connected insertion.

A. Disconnected insertions

The disconnected insertion [Fig. 1(b)] entails the correlation between the quark loops with up, down, and strange quark currents and the nucleon two-point propagators as discussed in Sec. II B. We consider the up and down to have the same mass so that their moments are the same.

1. First moments

First, we will discuss the results for the first moments from the $\mathcal{O}_{4i}(i = 1, 2, 3)$ operator for the case where the valence quarks in the nucleon propagators and the sea quark in the loop are the same. This is the case, when extrapolated to the physical u/d quark mass would give the

TABLE VI. Table for the values of $\langle x \rangle$ (D.I.) at $\kappa_v = \kappa_{\text{sea}} = 0.154$ for the $\mathcal{O}_{4i}$ operator by using five different methods.

Methods	*Fitting Range*	*No Subtraction*	4 *Subtractions*
Summation from 5 to 20	10–14	0.011 ± 0.019	0.030 ± 0.012
Summation from source to sink time	10–14	0.007 ± 0.013	0.029 ± 0.009
R. Lewis *et al.* [49]	11–14	0.000 ± 0.012	0.027 ± 0.009
Summation from (source time +1) to (sink time +1)	10–14	−0.002 ± 0.014	0.026 ± 0.010
Current analysis	10–14	0.004 ± 0.012	0.028 ± 0.008

TABLE VII. $\langle x \rangle$ (D.I.) for up (down) and strange quarks at various κ's and the linearly extrapolated results to the chiral limit with different number of nucleon sources for $\mathcal{O}_{4i}$ operator.

		1 source (No sub)	1 source (4 sub)	4 sources (4 sub)	16 sources (4 sub)
$\langle x \rangle_{u,d}$ (D.I.)	$\kappa_v = \kappa_{\rm sea} = 0.154$	0.004 ± 0.012	0.028 ± 0.008	0.013 ± 0.005	0.016 ± 0.003
	$\kappa_v = \kappa_{\rm sea} = 0.155$	0.009 ± 0.017	0.037 ± 0.012	0.018 ± 0.007	0.022 ± 0.004
	$\kappa_v = \kappa_{\rm sea} = 0.1555$	0.011 ± 0.022	0.044 ± 0.014	0.021 ± 0.008	0.025 ± 0.005
	Linear Extrapolation	0.033 ± 0.058	0.056 ± 0.019	0.028 ± 0.011	0.032 ± 0.006
$\langle x \rangle_{s+\bar{s}}$ (D.I.)	$\kappa_v = 0.154$, $\kappa_{\rm sea} = 0.154$	0.004 ± 0.012	0.028 ± 0.008	0.013 ± 0.005	0.016 ± 0.003
	$\kappa_v = 0.155$, $\kappa_{\rm sea} = 0.154$	0.005 ± 0.017	0.034 ± 0.011	0.016 ± 0.006	0.020 ± 0.004
	$\kappa_v = 0.1555$, $\kappa_{\rm sea} = 0.154$	0.004 ± 0.021	0.038 ± 0.014	0.017 ± 0.008	0.023 ± 0.004
	Linear Extrapolation	0.005 ± 0.029	0.046 ± 0.018	0.021 ± 0.010	0.027 ± 0.006
$\frac{\langle x \rangle_{s+\bar{s}}}{\langle x \rangle_{u+\bar{u}}}$		0.69 ± 0.64	0.85 ± 0.13	0.95 ± 0.18	0.88 ± 0.07

disconnected insertion result for the u and d quarks. We average over the three spatial directions on each configuration. From now on, $\mathcal{O}_{4i}$ stands for the average over 1, 2 and 3 directions.

We now consider the cases with equal valence and sea quark masses, i.e. $\kappa_v = \kappa_{\rm sea} = 0.154$, 0.155, and 0.1555 in order to extrapolate to the chiral limit to obtain $\langle x \rangle_{u+\bar{u}} = \langle x \rangle_{d+\bar{d}} = \langle x \rangle_{u,d}$ (D.I.). In Figs. 6(a)–6(c) we plot the ratios in Eq. (25) against the nucleon sink time t_2. The insertion time is summed from [source time +1] (i.e. $t_0 + 1$) to [sink time −1] (i.e. $t_2 - 1$). In these figures, we see that, after the unbiased subtraction of four terms, there is a clear straight line behavior starting from the time slice 10. On the other hand, without the unbiased subtraction, there is not a clear signal. In fact, they are consistent with zero slopes. Also, the plots show that the error bars get reduced after subtraction by a factor of ~1.5. To extract the values of $\langle x \rangle_{u,d}$ at each κ_v, we have performed a correlated fit of the slopes between the time slices 10 and 14. It gives us the value of the $\langle x \rangle_{u,d}$ (D.I.) at the corresponding κ_v. The values of $\langle x \rangle_{u,d}$ (D.I.), along with their errors, are listed in Table VII.

In chiral perturbation theory, the first moment of $\langle x \rangle$ has a leading nonanalytic behavior $\propto m_\pi^2 \ln(m_\pi^2/\mu^2)$ and leading analytic behavior $\propto m_\pi^2$ [68–71]. Since our pion masses are relatively heavy, we do not expect to be in the region where the nonanalytic behavior is important. Furthermore, our present calculation is based on the quenched approximation. In view of this and other systematic errors that we have not taken into account, such as the large volume limit and continuum limit, we shall take the conservative linear extrapolation of $\langle x \rangle_{u,d}$ to the chiral limit with the form $A + Bm_q a$ [Fig. 6(d)]. This linear extrapolation will inevitably introduce systematic errors. This issue will be dealt with when the configurations with lighter quark masses are available. We will certainly include the nonanalytic behavior when the results from the PAC-CS 2 + 1-flavor dynamical clover fermion configurations are available with lighter sea quark masses [72]. Before extrapolation, we have converted the values of $\langle x \rangle_{u,d}$ (D.I.) to those of tadpole-improved values by using the factors in Eq. (46).

We did the similar analysis for the cases with 4 and 16 nucleon sources. Figure 7 shows the ratios between three-point to two-point functions for all the sources with 4 subtractions, and Fig. 8(a) shows the linear extrapolation to the chiral limit. In Table VII, we list the renormalized and linearly extrapolated values (to the chiral limit) of $\langle x \rangle_{u,d}$ along with their errors. As stated in Eq. (45), the renormalization factor for this operator is 0.972. We find that the values for $\langle x \rangle_{u,d}$ are about 3σ away from zero for one and four sources and more than 5σ for 16 sources. We consider this a solid affirmation that we have been able to calculate the D.I. of $\langle x \rangle_{u,d}$ via the noise method.

Next, we consider the strange quark loop. This time we have fixed $\kappa_{\rm sea} = 0.154$ which corresponds to the strange quark mass. In Figs. 9(a)–9(c), we have plotted the ratio in Eq. (25) against the nucleon sink time by using the valence quark masses at $\kappa_v = 0.154$, 0.155, and 0.1555, respectively. A similar procedure has been followed as for the up (down) currents to obtain the slopes, which gives the values of $\langle x \rangle_{s+\bar{s}}$. Again, from these figures, it is clear that if we do

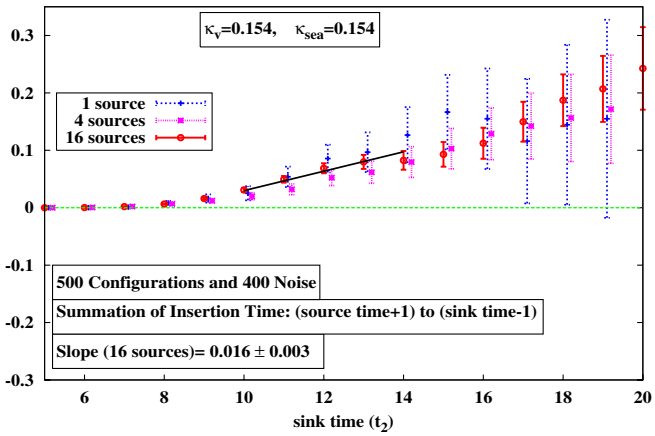

FIG. 7 (color online). The ratio of the three-point to two-point functions for the $\mathcal{O}_{4i}$ operator is plotted against the nucleon sink time (t_2) at $\kappa_{\rm sea} = 0.154$ and $\kappa_v = 0.154$ for 1, 4, and 16 sources after 4 subtractions.

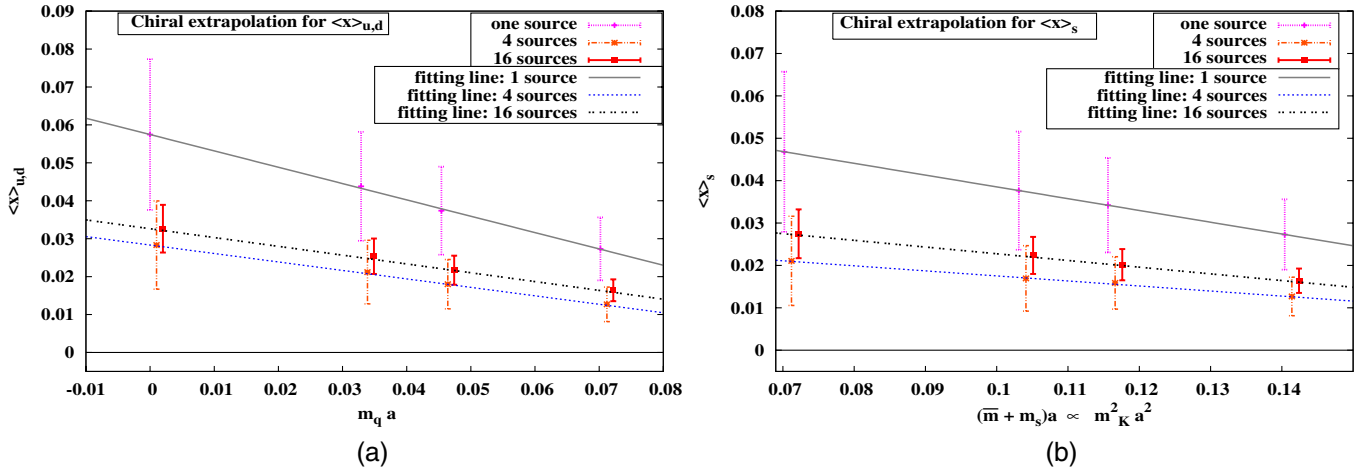

FIG. 8 (color online). Linear extrapolation to the chiral limit for the first moment with 1, 4, and 16 nucleon sources (a) for $\langle x \rangle_{u,d}$ (D.I.), and (b) for $\langle x \rangle_{s+\bar{s}}$ (D.I.).

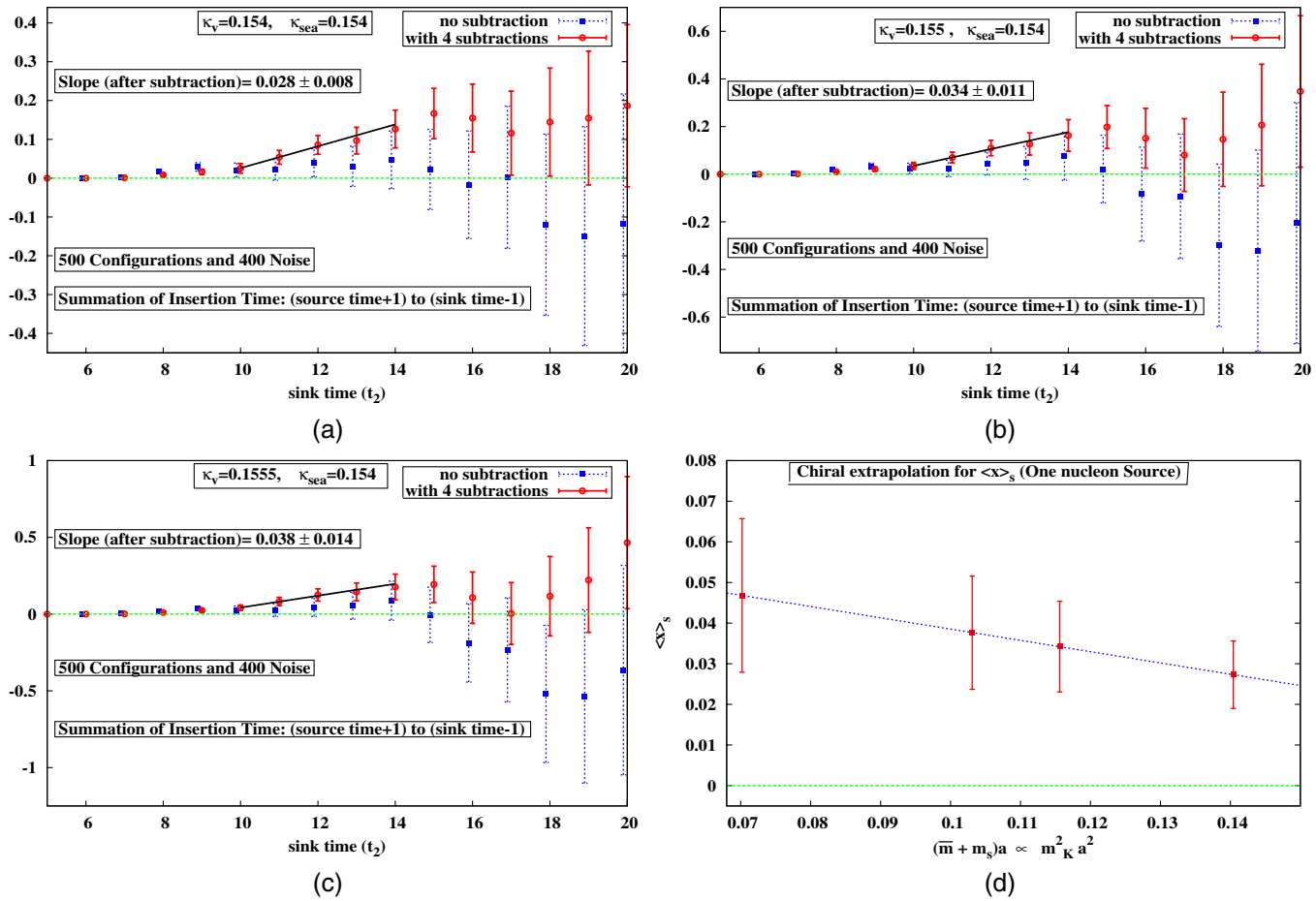

FIG. 9 (color online). The ratio of the three-point to two-point functions (summed over insertion time) for the $\mathcal{O}_{4i}$ operator, for the strange quark which is fixed at $\kappa_{\text{sea}} = 0.154$, is plotted against the nucleon sink time (t_2) at (a) $\kappa_v = 0.154$ and $\kappa_{\text{sea}} = 0.154$, (b) $\kappa_v = 0.155$ and $\kappa_{\text{sea}} = 0.154$, and (c) $\kappa_v = 0.1555$ and $\kappa_{\text{sea}} = 0.154$. (d) is a linear extrapolation of the valence quarks to the chiral limit for the first moment, $\langle x \rangle_{s+\bar{s}}$ (D.I.) of the strange quarks, plotted against $(\bar{m} + m_s)a$.

TABLE VIII. Table for the values of $\langle x \rangle$ (D.I.) for up (down) and strange quarks at various kappa values and after linear extrapolation to the chiral limit with different number of nucleon sources for the $\mathcal{O}_{44} - \frac{1}{3}(\mathcal{O}_{11} + \mathcal{O}_{22} + \mathcal{O}_{33})$ operator.

		1 source (No sub)	1 source (4 sub)	4 sources (4 sub)	16 sources (4 sub)
$\langle x \rangle_{u,d}$ (D.I.)	$\kappa_v = \kappa_{\text{sea}} = 0.154$	0.045 ± 0.044	0.033 ± 0.040	0.025 ± 0.026	0.038 ± 0.020
	$\kappa_v = \kappa_{\text{sea}} = 0.155$	0.075 ± 0.056	0.059 ± 0.053	0.032 ± 0.035	0.046 ± 0.027
	$\kappa_v = \kappa_{\text{sea}} = 0.1555$	0.095 ± 0.065	0.073 ± 0.060	0.034 ± 0.042	0.049 ± 0.033
	Linear Extrapolation	0.130 ± 0.081	0.095 ± 0.071	0.037 ± 0.050	0.058 ± 0.043
$\langle x \rangle_{s+\bar{s}}$ (D.I.)	$\kappa_v = 0.154$, $\kappa_{\text{sea}} = 0.154$	0.045 ± 0.044	0.033 ± 0.040	0.025 ± 0.026	0.038 ± 0.020
	$\kappa_v = 0.155$, $\kappa_{\text{sea}} = 0.154$	0.067 ± 0.056	0.047 ± 0.050	0.026 ± 0.034	0.041 ± 0.027
	$\kappa_v = 0.1555$, $\kappa_{\text{sea}} = 0.154$	0.087 ± 0.065	0.062 ± 0.057	0.026 ± 0.039	0.041 ± 0.033
	Linear Extrapolation	0.114 ± 0.080	0.077 ± 0.068	0.026 ± 0.048	0.043 ± 0.042

not use unbiased subtraction, we will not see a signal. The error bars get reduced after subtraction. The linear extrapolation to the chiral limit is performed with the form $A + B(\bar{m} + m_s)$ where $(\bar{m} + m_s) \propto m_K^2$, with $\bar{m}$ being the average of the up and down quark masses and m_s being the strange mass. In Table VII, we have listed values of $\langle x \rangle_{s+\bar{s}}$ (D.I.) for different κ_v's and fixed κ_{sea}. Also listed are the linearly extrapolated values of $\langle x \rangle_{s+\bar{s}}$ (D.I.) to the chiral limit. Again, we find that the value for $\langle x \rangle_{s+\bar{s}}$ is 4.5σ away from zero for 16 sources. We have also listed the ratio of $\langle x \rangle_{s+\bar{s}}$ (D.I.) to $\langle x \rangle_{u+\bar{u}}$ (D.I.) in Table VII. We see that the ratio is close to 1 as expected [36]. We should point out the

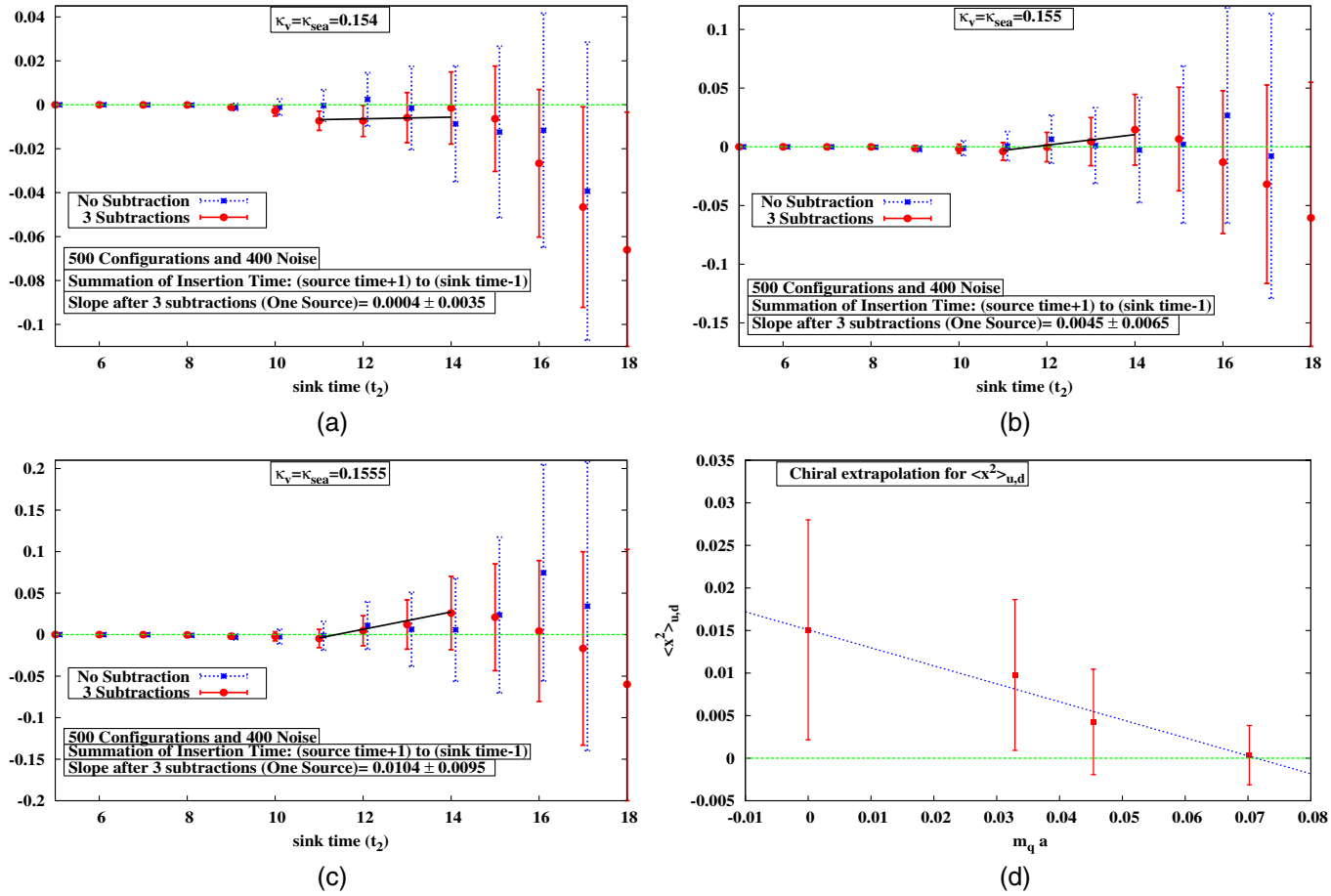

FIG. 10 (color online). The ratio of the three-point to two-point functions (summed over insertion time) of the $\mathcal{O}_{4ii} - \frac{1}{2}(\mathcal{O}_{4jj} + \mathcal{O}_{4kk})$ operator, for up (down), is plotted against the nucleon sink time t_2 at (a) $\kappa_v = \kappa_{\text{sea}} = 0.154$, (b) $\kappa_v = \kappa_{\text{sea}} = 0.155$, and (c) $\kappa_v = \kappa_{\text{sea}} = 0.1555$. (d) is the linear extrapolation to the chiral limit for the second moment, $\langle x^2 \rangle_{u,d}$ (D.I.) of the up (down) quarks, plotted against $m_q a$.

caveat that these results are based on the linear extrapolation to the chiral limit which are subjected to systematic corrections as mentioned above. The ratio is expected to be less susceptible to the systematic errors except the chiral extrapolation due to the nonanalytic terms. In view of the fact that the lattice calculations of both the $\langle x\rangle_{u+d}$ and $\langle x\rangle_{u-d}$ for the connected insertions at quark masses between the strange and the physical u/d mass are all larger than the respective experimental results (see Table XII in Sec. VI B), we expect the ratio of $\langle x\rangle_{s+\bar{s}}$ (D.I.) to $\langle x\rangle_{u+\bar{u}}$ (D.I.) for the physical u/d mass to be larger than that obtained with a linear extrapolation to the chiral limit.

We have performed the same analysis for the $\mathcal{O}_{44} - \frac{1}{3} \times (\mathcal{O}_{11} + \mathcal{O}_{22} + \mathcal{O}_{33})$ operator as in the case of the $\mathcal{O}_{4i}$ operator. The only difference is that we have used the nucleon with zero momentum in this case. But, due to the subtraction of the spatial trace terms in the current, it has significant numerical cancellations resulting in large statistical errors [26,28]. The error bar of the slope is $\sim 3 - 7$ times larger than that of $\mathcal{O}_{4i}$ operator. Because of this large error, the signal is only $\sim 1\sigma$ to 1.5σ away from zero shown in Table VIII. This happens for both $\langle x\rangle_{s+\bar{s}}$ and $\langle x\rangle_{u,d}$ (D.I.) for this operator.

2. Second moments

We will now present the results for the second moments obtained by using the current $\mathcal{O}_{4ii} - \frac{1}{2}(\mathcal{O}_{4jj} + \mathcal{O}_{4kk})(i \neq j \neq k; i, j, k = 1, 2, 3)$ for up (down) and strange quarks (see Figs. 10–13). We average over the results from the three operators: $\mathcal{O}_{411} - \frac{1}{2}(\mathcal{O}_{422} + \mathcal{O}_{433})$, $\mathcal{O}_{422} - \frac{1}{2}(\mathcal{O}_{433} + \mathcal{O}_{411})$, and $\mathcal{O}_{433} - \frac{1}{2}(\mathcal{O}_{411} + \mathcal{O}_{422})$. So $\mathcal{O}_{4ii} - \frac{1}{2} \times (\mathcal{O}_{4jj} + \mathcal{O}_{4kk})$ will mean average over 1, 2 and 3 directions from now on. In addition, we have used three subtraction terms (κD, $\kappa^2 D^2$, and $\kappa^3 D^3$). For this operator, we have performed the same analysis as for the operators for the first moments, with the fitting done from $t_2 = 11$ to 14. The values are presented in Table IX. Unfortunately, we did not see any clear signal either for $\langle x^2\rangle_{u,d} (= \langle x^2\rangle_{u-\bar{u}} = \langle x^2\rangle_{d-\bar{d}})$ or for $\langle x^2\rangle_{s-\bar{s}}$, even with unbiased subtractions and multiples sources. The statistical errors are large and the error bars overlap either with zero or the signal is at best 1σ to

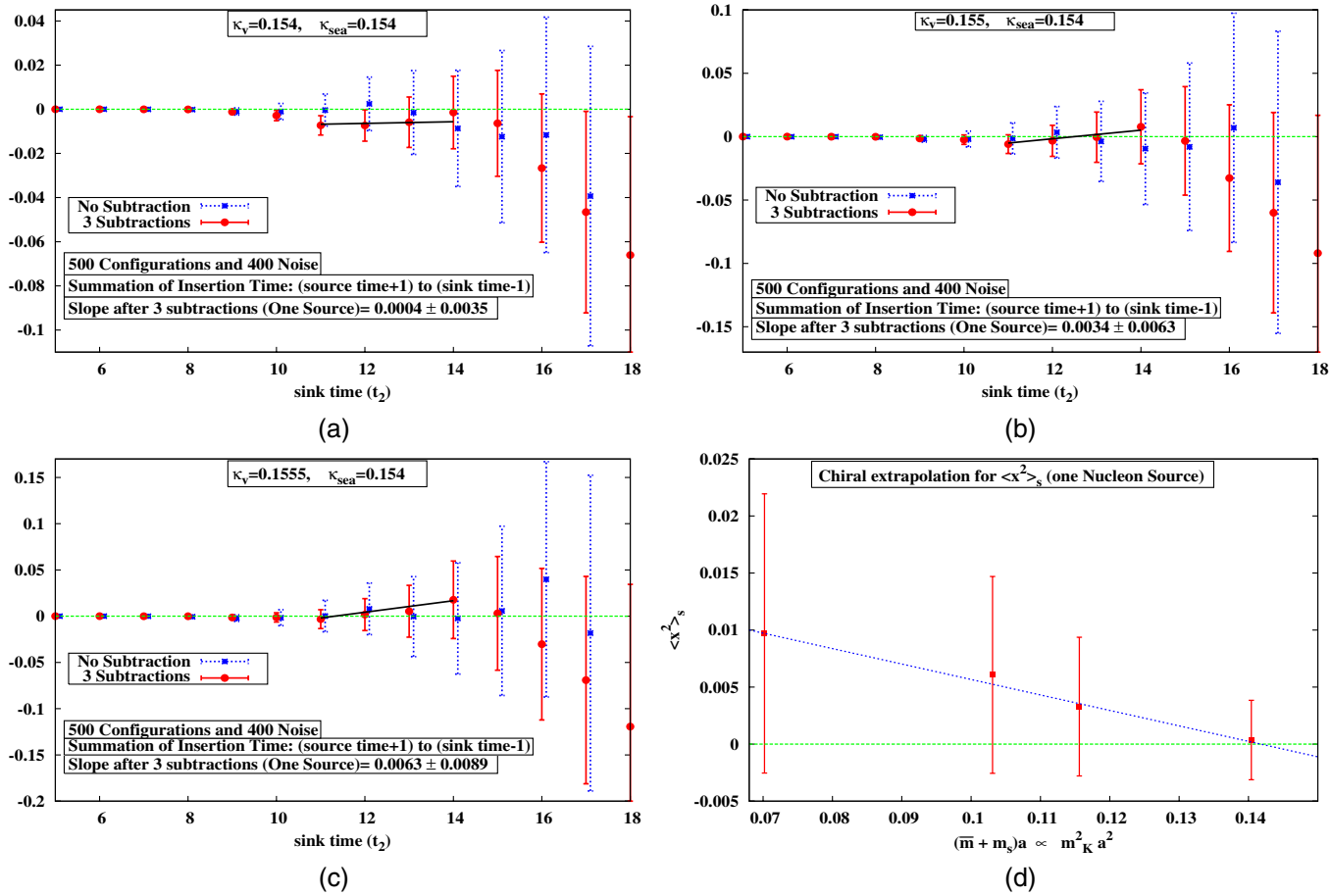

FIG. 11 (color online). The ratio of the three-point to two-point functions (summed over insertion time) of the $\mathcal{O}_{4ii} - \frac{1}{2}(\mathcal{O}_{4jj} + \mathcal{O}_{4kk})$ operator, for strange quarks, is plotted against the nucleon sink time t_2 at (a) $\kappa_v = 0.154$ and $\kappa_{\rm sea} = 0.154$, (b) $\kappa_v = 0.155$ and $\kappa_{\rm sea} = 0.154$, and (c) $\kappa_v = 0.1555$ and $\kappa_{\rm sea} = 0.154$. (d) is the linear extrapolation to the chiral limit for the second moment, $\langle x^2\rangle_{s-\bar{s}}$ (D.I.), of the strange quarks, plotted against $(\bar{m} + m_s)a$.

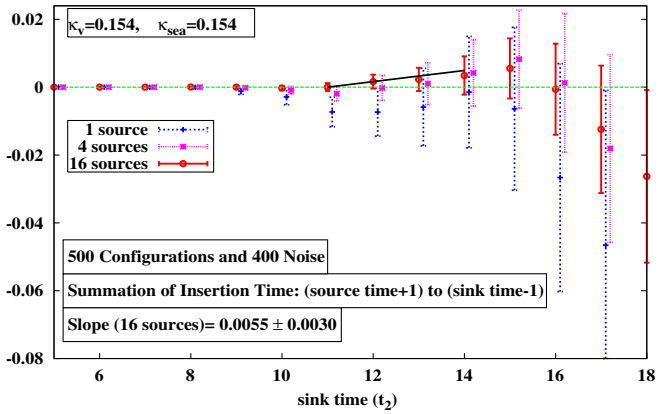

FIG. 12 (color online). The ratio of the three-point to two-point functions for the $\mathcal{O}_{4ii} - \frac{1}{2}(\mathcal{O}_{4jj} + \mathcal{O}_{4kk})$ operator is plotted against the nucleon sink time t_2 at $\kappa_v = 0.154$ and $\kappa_{\rm sea} = 0.154$ for 1, 4, and 16 sources after 3 subtractions.

1.5σ away from zero for various nucleon sources. For the best case (16 nucleon sources), the range for $\langle x^2\rangle_{u,d}$ is [0.0035, 0.0127] and that for $\langle x^2\rangle_{s-\bar{s}}$ is [0.0016, 0.0102]. We conclude that they are consistent with zero in the present calculation.

B. Connected insertions

In this section, we will present the results for the first and second moments for the case of connected insertions. We will consider both up and down quark currents. Unlike in D.I., they are different in the case of C.I. As stated earlier, we consider nucleon momentum in the x-direction only and we fix the nucleon sink time at $t_2 = 16$.

1. First moments

First, we will discuss the results for the first moments by using the current $\mathcal{O}_{41}$ for up quarks. In Figs. 14(a)–14(c), we plot the ratio in Eq. (22) against the current insertion time t_1 for $\kappa_v = 0.154$, 0.155, and 0.1555, respectively. In these figures, we see that there is a plateau region from the time slice 9 to 13. To extract the values of $\langle x\rangle_{u+\bar{u}}$ (C.I.) at each κ_v, we fit a constant between the time slice 9 to 13. These values and the corresponding errors are listed in Table X.

After obtaining $\langle x\rangle_{u+\bar{u}}$ (C.I.) at finite quark mass, we then linearly extrapolate the valence quarks to the chiral limit. Before extrapolation, we have converted the values of $\langle x\rangle_{u+\bar{u}}$ (C.I.) to those of tadpole-improved values by using the factors in Eq. (46). As in the case of $\langle x\rangle_{u,d}$ (D.I.), we have extrapolated with the form $A + Bm_q a$. In Table X,

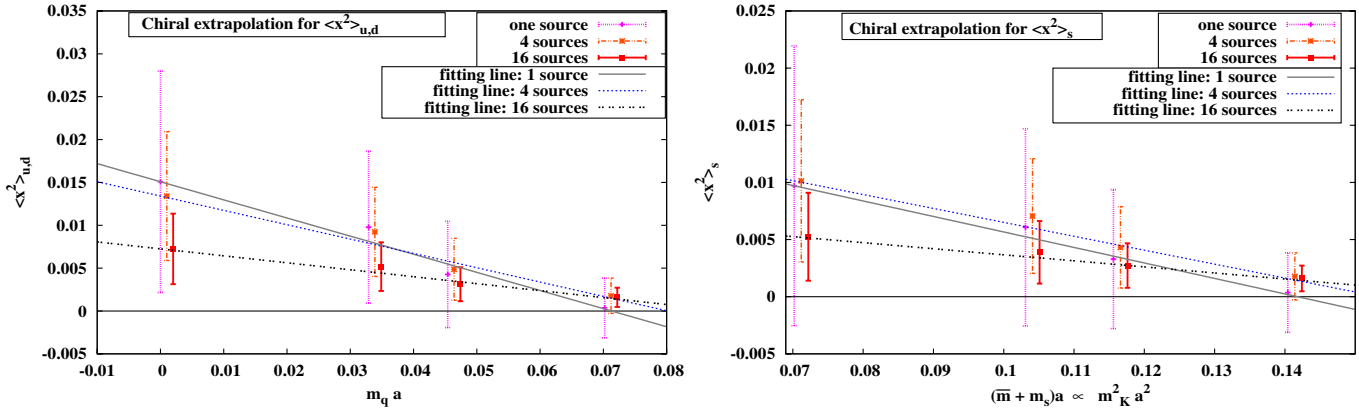

FIG. 13 (color online). Linear extrapolation to the chiral limit for the second moment with 1, 4, and 16 nucleon sources (a) for $\langle x^2\rangle_{u,d}$, (D.I.), and (b) for $\langle x^2\rangle_{s-\bar{s}}$ (D.I.).

TABLE IX. $\langle x^2\rangle$ (D.I.) for up (down) and strange quarks at various κ's and the linearly extrapolated results to the chiral limit with different number of nucleon sources.

		1 source (No Sub)	1 source (4Sub)	4 sources (4Sub)	16 sources (4Sub)
$\langle x^2\rangle_{u,d}$ (D.I.)	$\kappa_v = \kappa_{\rm sea} = 0.154$	0.0020 ± 0.0060	0.0004 ± 0.0035	0.0018 ± 0.0021	0.015 ± 0.0011
	$\kappa_v = \kappa_{\rm sea} = 0.155$	0.0056 ± 0.0098	0.0043 ± 0.0620	0.0049 ± 0.0036	0.0031 ± 0.0020
	$\kappa_v = \kappa_{\rm sea} = 0.1555$	0.0122 ± 0.0133	0.0098 ± 0.0089	0.0092 ± 0.0052	0.0052 ± 0.0028
	Linear Extrapolation	0.0195 ± 0.0213	0.0168 ± 0.0144	0.0150 ± 0.0084	0.0081 ± 0.0046
$\langle x^2\rangle_{s-\bar{s}}$ (D.I.)	$\kappa_v = 0.154$, $\kappa_{\rm sea} = 0.154$	0.0020 ± 0.0060	0.0004 ± 0.0035	0.0018 ± 0.0021	0.015 ± 0.0011
	$\kappa_v = 0.155$, $\kappa_{\rm sea} = 0.154$	0.0048 ± 0.0099	0.0033 ± 0.0061	0.0043 ± 0.0036	0.010 ± 0.0071
	$\kappa_v = 0.1555$, $\kappa_{\rm sea} = 0.154$	0.0086 ± 0.0134	0.0061 ± 0.0086	0.0071 ± 0.0050	0.0039 ± 0.0027
	Linear Extrapolation	0.0132 ± 0.0210	0.0108 ± 0.0137	0.0113 ± 0.0079	0.0059 ± 0.0043

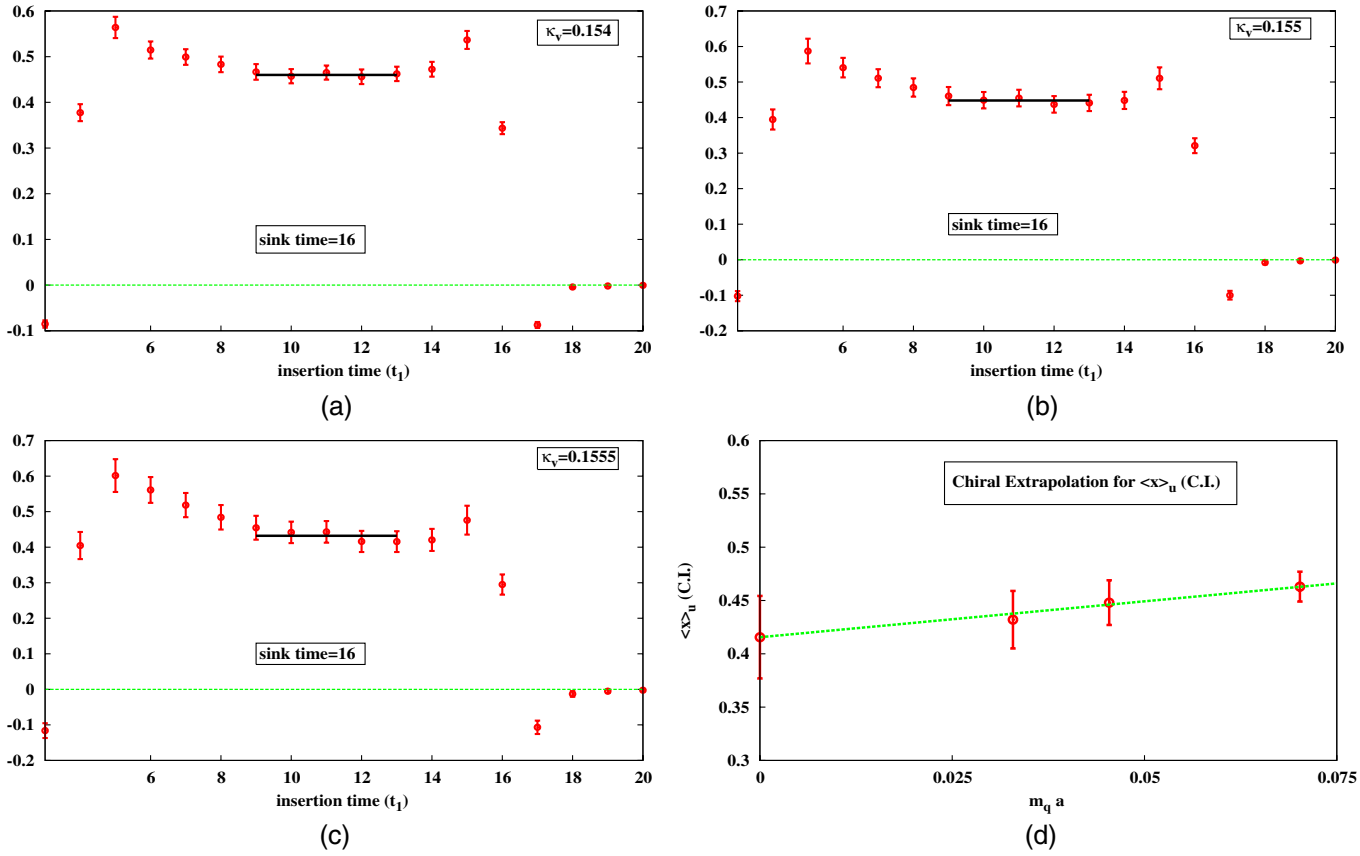

FIG. 14 (color online). The ratio of the three-point to two-point functions (C.I.), with fixed sink time at $t_2 = 16$, for the $\mathcal{O}_{41}$ operator, for up quarks, is plotted against the current insertion time (t_1) at (a) $\kappa_v = 0.154$, (b) $\kappa_v = 0.155$, and (c) $\kappa_v = 0.1555$. (d) is a linear extrapolation to the chiral limit plotted against $m_q a$.

we have listed the renormalized linearly extrapolated value of $\langle x \rangle_{u+\bar{u}}$ (C.I.). As stated in Eq. (45), the renormalization factor for this operator is 0.972.

Next, we consider the current for the down quark [Figs. 15(a)–15(d)]. Similar procedure is followed as for the up quarks to obtain the constants, which give the values of $\langle x \rangle_{d+\bar{d}}$'s. Again, the fitting is performed from the insertion time 9 to 13. The values of $\langle x \rangle_{d+\bar{d}}$'s and their corresponding errors are listed in Table X.

Now, we will consider the current $\mathcal{O}_{44} - \frac{1}{3} \times (\mathcal{O}_{11} + \mathcal{O}_{22} + \mathcal{O}_{33})$ for both up [Figs. 16(a)–16(d)] and down quarks [Figs. 17(a)–17(d).] The fitting is performed from the insertion time 9 to 11 for both up and down quark currents. The values of the $\langle x \rangle_{u+\bar{u}}$ and $\langle x \rangle_{d+\bar{d}}$ (C.I.) for this operator, along with their errors, are listed in Table X. The renormalization factor for this current is 0.953 as obtained from Eq. (45).

2. Second moment

For the second moment, we consider the operator $\mathcal{O}_{411} - \frac{1}{2}(\mathcal{O}_{422} + \mathcal{O}_{433})$ for both the up [Figs. 18(a)–18(d)] and

TABLE X. Table for the values of $\langle x \rangle$ (C.I.) for up and down quarks at various kappa values and after linear extrapolation to the chiral limit for the $\mathcal{O}_{41}$ and $\mathcal{O}_{44} - \frac{1}{3}(\mathcal{O}_{11} + \mathcal{O}_{22} + \mathcal{O}_{33})$ operators.

$\langle x \rangle^{41}_{u+\bar{u}}$ (C.I.)	$\kappa_v = 0.154$	0.463 ± 0.014
	$\kappa_v = 0.155$	0.448 ± 0.021
	$\kappa_v = 0.1555$	0.432 ± 0.027
	Linear Extrapolation	0.408 ± 0.038
$\langle x \rangle^{41}_{d+\bar{d}}$ (C.I.)	$\kappa_v = 0.154$	0.193 ± 0.007
	$\kappa_v = 0.155$	0.179 ± 0.011
	$\kappa_v = 0.1555$	0.168 ± 0.014
	Linear Extrapolation	0.148 ± 0.019
$\langle x \rangle^{44}_{u+\bar{u}}$ (C.I.)	$\kappa_v = 0.154$	0.491 ± 0.013
	$\kappa_v = 0.155$	0.466 ± 0.019
	$\kappa_v = 0.1555$	0.458 ± 0.025
	Linear Extrapolation	0.420 ± 0.035
$\langle x \rangle^{44}_{d+\bar{d}}$ (C.I.)	$\kappa_v = 0.154$	0.224 ± 0.007
	$\kappa_v = 0.155$	0.209 ± 0.010
	$\kappa_v = 0.1555$	0.203 ± 0.013
	Linear Extrapolation	0.181 ± 0.018

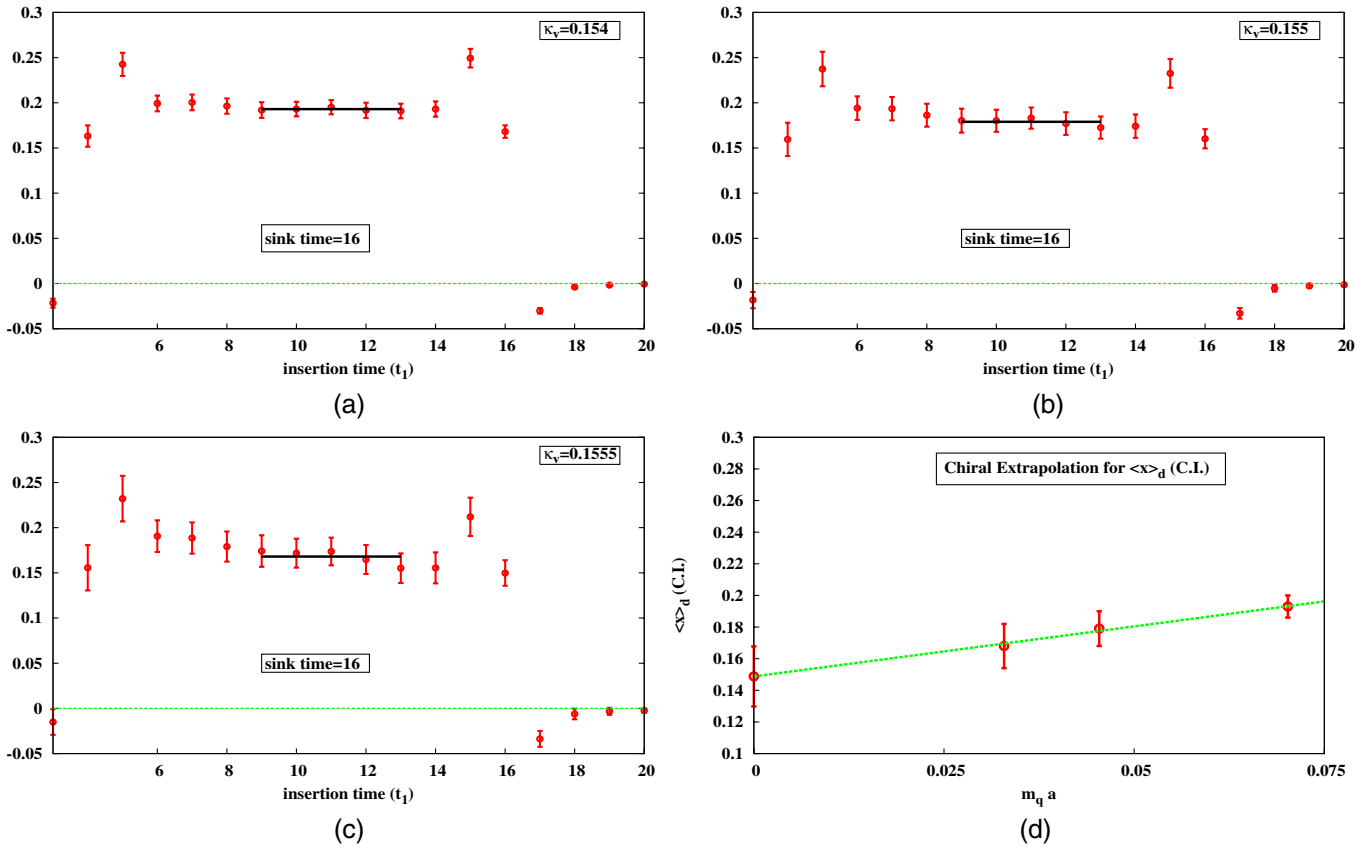

FIG. 15 (color online). The ratio of the three-point to two-point functions (C.I.), with fixed sink time at $t_2 = 16$, for the $\mathcal{O}_{41}$ operator, for down quarks, is plotted against the current insertion time (t_1) at (a) $\kappa_v = 0.154$, (b) $\kappa_v = 0.155$, and (c) $\kappa_v = 0.1555$. (d) is a linear extrapolation to the chiral limit plotted against $m_q a$.

down [Figs. 19(a)–19(d)] quarks. We did the similar analysis as in the case of the first moments. The fitting is performed from the insertion time 9 to 11 for both up and down quark currents. The values of the $\langle x^2\rangle_{u-\bar{u}}$ and $\langle x^2\rangle_{d-\bar{d}}$ (C.I.) for this operator, along with their errors, are listed in Table XI. The renormalization factor for this current is 1.116 which we have obtained from Eq. (45).

We list our results in comparison with those from previous calculations in Table XII. Except for our calculations, other groups have averaged the results of the first moments obtained from the two operators $\mathcal{O}_{41}$ and $\mathcal{O}_{44} - \frac{1}{3}(\mathcal{O}_{11} + \mathcal{O}_{22} + \mathcal{O}_{33})$. As we can see, all the results agree with each other within errors.

TABLE XI. Table for the values of $\langle x^2\rangle^{411}$(C.I.) for up and down quarks at various kappa values and after linear extrapolation to the chiral limit for the $\mathcal{O}_{411} - \frac{1}{2}(\mathcal{O}_{422} + \mathcal{O}_{433})$ operator.

$\langle x^2\rangle^{411}_{u-\bar{u}}$ (C.I.)	$\kappa_v = 0.154$	0.128 ± 0.007
	$\kappa_v = 0.155$	0.124 ± 0.010
	$\kappa_v = 0.1555$	0.122 ± 0.013
	Linear Extrapolation	0.117 ± 0.018
$\langle x^2\rangle^{411}_{d-\bar{d}}$ (C.I.)	$\kappa_v = 0.154$	0.0504 ± 0.0035
	$\kappa_v = 0.155$	0.0500 ± 0.0050
	$\kappa_v = 0.1555$	0.0532 ± 0.0066
	Linear Extrapolation	0.0521 ± 0.0091

For the QCDSF calculations at $\mu = 5$ GeV^2 (second column), the reported values of $\langle x\rangle$ are the averages of two different procedures in [73,74], whereas, the result of $\langle x^2\rangle$ is obtained from [74]. For both procedures, two different lattices ($16^3 \times 32$ and $24^3 \times 32$) are used for several κ values. For the $16^3 \times 32$ lattice, the number of gauge configurations involved is $O(1000)$ and for the $24^3 \times 32$ lattice, the number of gauge configurations involved is $O(100)$. All the calculations are performed for $\beta = 6.0$. For the calculations at $\mu = 4$ GeV^2 [75] (third column), three κ values, 0.155, 0.153, and 0.1515, are used on a $16^3 \times 32$ lattice. The number of independent gauge configurations involved are 100, 600, and 400 at these κ values, respectively. All the calculations are performed for $\beta = 6.0$ by using standard Wilson action in quenched approximation.

For the LHPC calculations at $\mu = 4$ GeV^2 (fourth column) [76], a $16^3 \times 32$ lattice is used for three κ values. The number of gauge configurations used are 200 at $\beta = 6.0$ for each of the three κ's in quenched approximation. LHPC

TABLE XII. Comparison of results for renormalized first and second moments (connected insertion) in the chiral limit with other lattice calculations and phenomenology in $\overline{\text{MS}}$ scheme.

Moments	Kentucky (quenched) ($\mu^2 = 4$ GeV^2)	QCDSF (quenched) ($\mu^2 \simeq 5$ GeV^2)	QCDSF (quenched) ($\mu^2 = 4$ GeV^2)	LHPC (quenched) ($\mu^2 = 4$ GeV^2)	LHPC (full QCD) ($\mu^2 = 4$ GeV^2)	Experiment CTEQ3M ($\mu^2 = 4$ GeV^2)
$\langle x\rangle^{41}_{u+\bar{u}}$	0.408 (38)	0.410(34)	0.452 (26)	0.454 (29)	0.459 (29)	0.284
$\langle x\rangle^{44}_{u+\bar{u}}$	0.420 (35)					
$\langle x\rangle^{41}_{d+\bar{d}}$	0.148 (19)	0.180 (16)	0.189 (12)	0.203 (14)	0.190 (17)	0.102
$\langle x\rangle^{44}_{d+\bar{d}}$	0.181 (18)					
$\langle x^2\rangle^{411}_{u-\bar{u}}$	0.117 (18)	0.108 (16)	0.104 (20)	0.119 (61)	0.176 (63)	0.083
$\langle x^2\rangle^{411}_{d-\bar{d}}$	0.052 (9)	0.036 (8)	0.037 (10)	0.029 (32)	0.031 (30)	0.025

calculations are also performed in full (unquenched) QCD on a $16^3 \times 32$ lattice. Four different κ's are used at $\beta = 5.6$ for 200 SESAM configurations and three different κ's are used at $\beta = 6.0$ for 100 SCRI configurations.

From this comparison, we see that our results are comparable with other lattice calculations. But all the lattice calculations for $\langle x\rangle_{u-d}$ which involves only the C.I. seem to be larger than the experimental result [83]. This is a well known problem and is presumably due to the fact that quark masses are still too heavy compared to the physical ones [77,78].

VII. CONCLUSION AND DISCUSSION

We have calculated the first and second moments of the proton's parton distribution functions for both the connected and disconnected insertions in lattice QCD. The lattice calculations are carried out on quenched $16^3 \times 24$

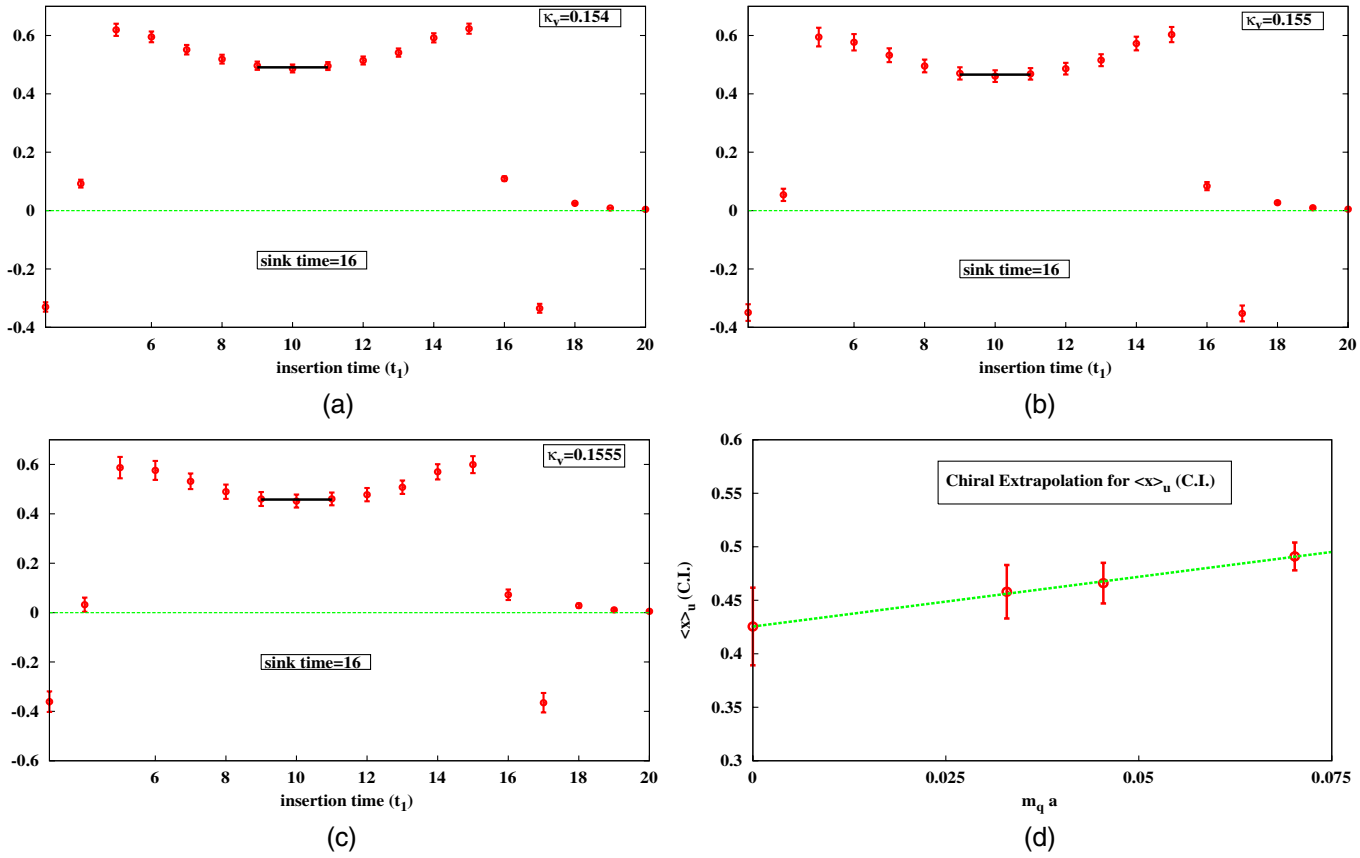

FIG. 16 (color online). The ratio of the three-point to two-point functions (C.I.), with fixed sink time at $t_2 = 16$, for the $\mathcal{O}_{44} - \frac{1}{3} \times (\mathcal{O}_{11} + \mathcal{O}_{22} + \mathcal{O}_{33})$ operator, for up quarks, is plotted against the current insertion time t_1 at (a) $\kappa_v = 0.154$, (b) $\kappa_v = 0.155$, and (c) $\kappa_v = 0.1555$. (d) is a linear extrapolation to the chiral limit plotted against $m_q a$.

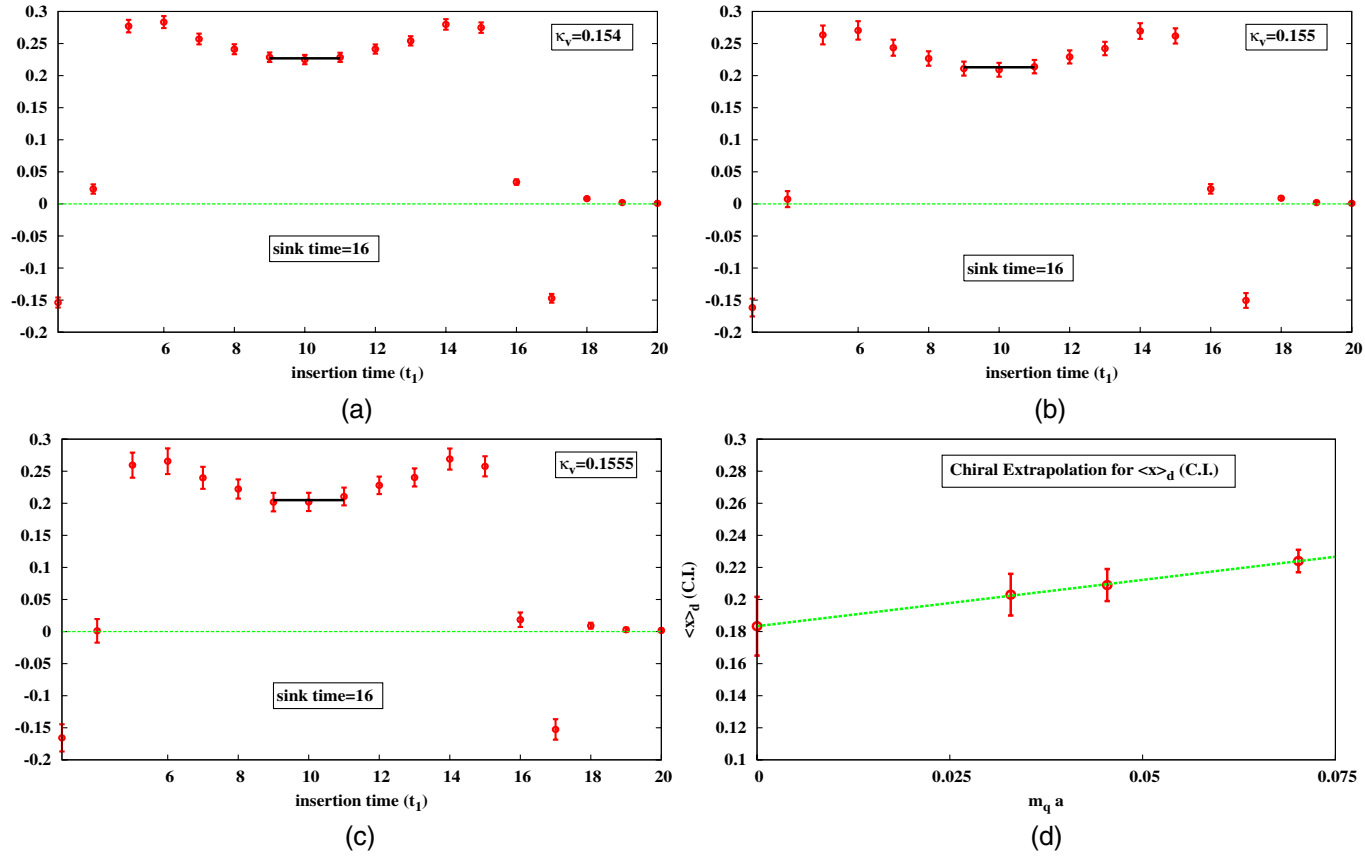

FIG. 17 (color online). The ratio of the three-point to two-point functions (C.I.), with fixed sink time at $t_2 = 16$, for the $\mathcal{O}_{44} - \frac{1}{3} \times (\mathcal{O}_{11} + \mathcal{O}_{22} + \mathcal{O}_{33})$ operator, for down quarks, is plotted against the current insertion time t_1 at (a) $\kappa_v = 0.154$, (b) $\kappa_v = 0.155$, and (c) $\kappa_v = 0.1555$. (d) is a linear extrapolation to the chiral limit plotted against $m_q a$.

lattices with $\beta = 6.0$ and quark masses which correspond to pion masses of 650(3), 538(4) and 478(4) MeV, and nucleon masses at 1291(9), 1159(11), and 1093(13) MeV, respectively. The physical results are obtained from linear extrapolation to the physical point (to the chiral limit). The connected insertion results turn out to be consistent with the previous quenched and full QCD calculations.

The calculation of the moments for the sea quark distribution in the D.I. is carried out for the first time. With 400 Z_2 noise, 500 gauge configurations, and with unbiased subtractions and 16 nucleon sources, we are able to obtain results with $\sim 5\sigma$ signals for the first moments. The result of $\langle x \rangle_s = 0.027 \pm 0.006$ can be used to constrain $\langle x \rangle_s$ in the phenomenological fitting of parton distribution functions which is uncertain in the range $0.018 < \langle x \rangle_s < 0.04$ [8]. More interestingly, we find that

$$\left. \frac{\langle x \rangle_{s+\bar{s}}}{\langle x \rangle_{u+\bar{u}}} \right|_{\text{D.I.}} = \left. \frac{\int dx x(s(x) + \bar{s}(x))}{\int dx x(u(x) + \bar{u}(x))} \right|_{\text{D.I.}} = 0.88 \pm 0.07, \tag{48}$$

which is about twice as large as the average phenomenological value from fitting the parton distribution functions to experiments [8]

$$\frac{\int dx x[s(x) + \bar{s}(x)]}{\int dx x[\bar{u}(x) + \bar{d}(x)]} \sim 0.27 - 0.67. \tag{49}$$

This difference is understandable and has been anticipated from the path-integral formulation of parton degrees of freedom [36]. The ratio in the lattice calculation involves u/d quarks in the disconnected insertion (quark loops) [79], while the phenomenological ratio involves the $\bar{u}(x) + \bar{d}(x)$ in the connected insertion as well. The discrepancy suggests that the momentum carried by the $\bar{u}/\bar{d}$ quarks are roughly equally shared in the connected sea and the disconnected sea. The fact that there is antiquark in the connected sea is demonstrated by the large $\bar{u}(x) - \bar{d}(x)$ difference from the Gottfried sum rule violation [37] which cannot be accommodated by the small u and d difference due to isospin breaking in the disconnected sea. The combined Gottfried sum rule violation and the discrepancy of the ratios in Eqs. (48) and (49) suggests the following form for the antiparton distribution functions [36]:

$$\begin{aligned} \bar{u}(x) &= a_0 x^{a_1}(1-x)^{a_2} + b_u x^{b_1}(1-x)^{b_2}, \\ \bar{d}(x) &= a_0 x^{a_1}(1-x)^{a_2} + b_d x^{b_1}(1-x)^{b_2}, \\ \bar{s}(x) &= a_s x^{a_1}(1-x)^{a_2}, \end{aligned} \tag{50}$$

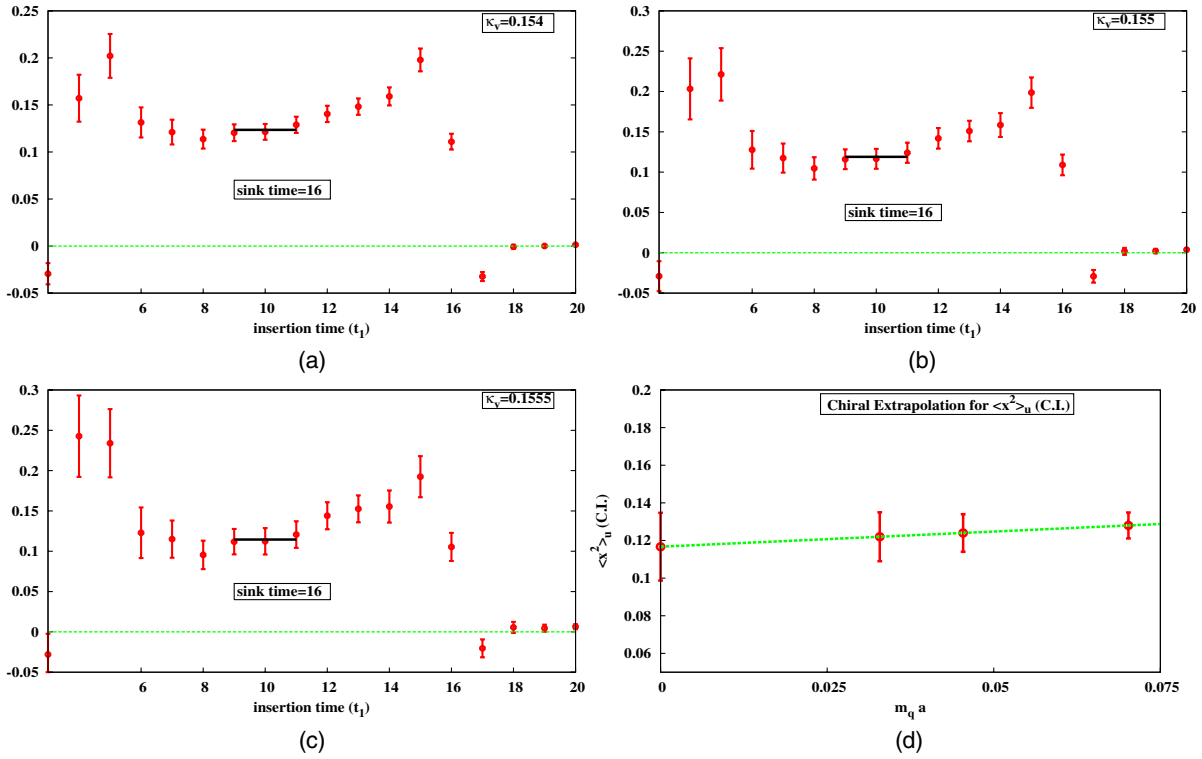

FIG. 18 (color online). The ratio of the three-point to two-point functions (C.I.), with fixed sink time at $t_2 = 16$, for the $\mathcal{O}_{411} - \frac{1}{2} \times (\mathcal{O}_{422} + \mathcal{O}_{433})$ operator, for up quarks, is plotted against the current insertion time (t_1) at (a) $\kappa_v = 0.154$, (b) $\kappa_v = 0.155$, and (c) $\kappa_v = 0.1555$. (d) is a linear extrapolation to the chiral limit plotted against $m_q a$.

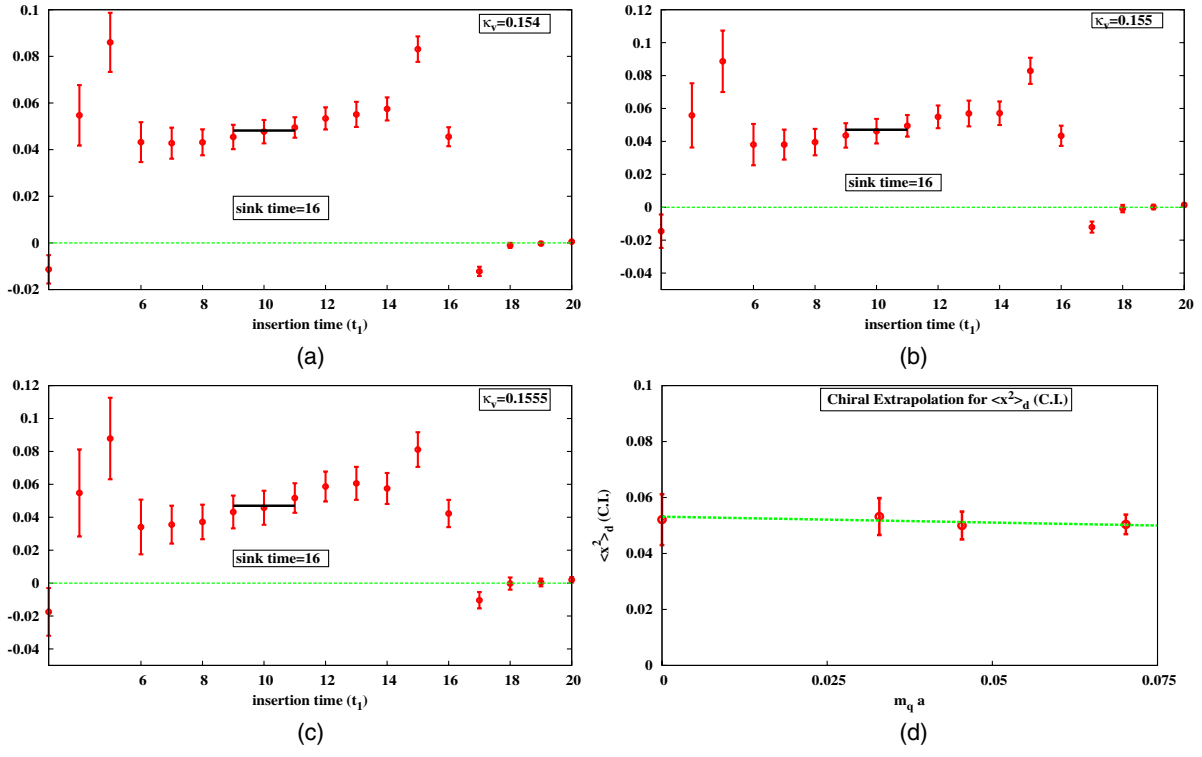

FIG. 19 (color online). The ratio of the three-point to two-point functions (C.I.), with fixed sink time at $t_2 = 16$, for the $\mathcal{O}_{411} - \frac{1}{2} \times (\mathcal{O}_{422} + \mathcal{O}_{433})$ operator, for down quarks, is plotted against the current insertion time t_1 at (a) $\kappa_v = 0.154$, (b) $\kappa_v = 0.155$, and (c) $\kappa_v = 0.1555$. (d) is a linear extrapolation to the chiral limit plotted against $m_q a$.

where the first terms are for the disconnected seas with Pomeron exchanges so that $a_1 \sim -1$ and the second terms are from the connected sea with Reggeon exchanges so that $b_1 \sim -\alpha_R$. The present lattice calculation suggests that $\frac{a_s}{a_0}$ can be constrained to the ratio in Eq. (48). We should emphasize that the current result is based on a quenched lattice calculation with linear chiral extrapolation from relatively heavy quarks. We should take it with a sizable grain of salt. As far as phenomenological fittings are concerned, the $\bar{u}(x) - \bar{d}(x)$ has been taken into account which has a small x behavior of $\sim x^{-1/2}$ [80]. However, the conventional ansatz $\bar{s}(x) \sim \bar{u}(x) + \bar{d}(x)$ used in recent fittings [8,9] is obviously inadequate [36]. One needs to differentiate the different small x behaviors in the connected sea and disconnected sea and fit the $\bar{u}(x)$, $\bar{d}(x)$, and $\bar{s}(x)$ accordingly.

We have made an attempt to calculate $\langle x^2 \rangle_s$ to see if it is $s(x)$ or $\bar{s}(x)$ which is leading in large x. Our result has a tendency to be positive, similar to the experimental tendency of $s_- = \int dx x(s(x) - \bar{s}(x))$ being positive, but it is consistent with zero within error. We will see if the signal is stronger with the inclusion of $2 + 1$ flavor dynamical fermions.

So far, our results are obtained in the quenched approximation with relatively large quark masses and small volume. They are subjected to large systematic errors. We will focus our attention next on the dynamical fermion calculation with $2 + 1$ flavor dynamical clover fermion configurations [81], and systematically move to smaller quark masses, larger volumes, and the continuum limit [82].

ACKNOWLEDGMENTS

The work was partially supported by U.S. DOE Grant No. DE-FG05-84ER40154. The research of M. Deka was supported in part by Graduate Student Research Assistantship from Thomas Jefferson National Accelerator Facility under Jefferson Lab-university affiliation related Nuclear Physics research. The research of N. Mathur is supported under the grant DST-SR/S2/RJN-19/2007, India. We would like to thank Andrei Alexandru, Devdatta Mankame, Ivan Horváth, and Anyi Li for their help and useful suggestions. The numerical computations were performed on the supercomputer at the Center for Computational Sciences, University of Kentucky.

APPENDIX A: THREE-POINT CORRELATION FUNCTIONS

1. General considerations

For the forward matrix elements, the three point-function for any general operator $\mathcal{O}$ (color and spin indices suppressed) is defined as

$$G^{\alpha\beta}_{N\mathcal{O}N}(t_2, t_1, \vec{p}) = \sum_{\vec{x}_2, \vec{x}_1} e^{-i\vec{p}.(\vec{x}_2 - \vec{x}_0)} \langle 0|\mathrm{T}(\chi^\alpha(x_2)\mathcal{O}(x_1) \times \bar{\chi}^\beta(x_0))|0\rangle, \tag{A1}$$

where $t = t_2$ is the nucleon sink time, $t = t_1$ is the current insertion time, $t = t_0$ is the nucleon source time, and $\vec{p}_i$ is the momentum of the nucleon, respectively. We now consider the following situations:

(i) When $t_2 > t_1 > t_0$, we get

$$\begin{aligned} G^{\alpha\beta}_{N\mathcal{O}N}(t_2, t_1, \vec{p}) &= \sum_{\vec{x}_2, \vec{x}_1} e^{-i\vec{p}.(\vec{x}_2 - \vec{x}_0)} \sum_{n_1, \vec{q}_1, s_1} \sum_{n_2, \vec{q}_2, s_2} \langle 0|\chi^\alpha(x_2)|n_2, \vec{q}_2, s_2\rangle\langle n_2, \vec{q}_2, s_2|\mathcal{O}(x_1)|n_1, \vec{q}_1, s_1\rangle\langle n_1, \vec{q}_1, s_1|\bar{\chi}^\beta(x_0)|0\rangle \\ &= N^2 \sum_s e^{-E_p^{0+}(t_2 - t_0)} \langle 0|\chi^\alpha(x_0)|0^+, \vec{p}, s\rangle\langle 0^+, \vec{p}, s|\mathcal{O}(x_0)|0^+, \vec{p}, s\rangle\langle 0^+, \vec{p}, s|\bar{\chi}^\beta(x_0)|0\rangle \\ &\quad + N^2 \sum_s e^{-E_p^{0-}(t_2 - t_0)} \langle 0|\chi^\alpha(x_0)|0^-, \vec{p}, s\rangle\langle 0^-, \vec{p}, s|\mathcal{O}(x_0)|0^-, \vec{p}, s\rangle\langle 0^-, \vec{p}, s|\bar{\chi}^\beta(x_0)|0\rangle \\ &\quad + \sum_{\theta=+,-} [e^{-E_p^{0(\theta)}(t_2 - t_1)} e^{-E_p^{1(\theta)}(t_1 - t_0)} C^{(\theta)(1)\alpha\beta}(\vec{p}) + e^{-E_p^{1(\theta)}(t_2 - t_1)} e^{-E_p^{0(\theta)}(t_1 - t_0)} C^{(\theta)(2)}(\vec{p})] \\ &\quad + \sum_{\theta, \theta'=+,-} \sum_{n_1^{(\theta)}, n_2^{(\theta')}=1}^{\infty} [e^{-E_p^{n_2^{(\theta')}}(t_2 - t_1)} e^{-E_p^{n_1^{(\theta)}}(t_1 - t_0)} f^{(1)\alpha\beta}(n_1^{(\theta)}, n_2^{(\theta')}, \vec{p})], \end{aligned} \tag{A2}$$

where N is the number of lattice sites, and the superscript $+$ ($-$) represents positive (negative) parity state.

$$\begin{aligned} C^{(\theta)(1)\alpha\beta}(\vec{p}) &= N^2\langle 0|\chi^\alpha(x_0)|0^{(\theta)}, \vec{p}, s\rangle\langle 0^{(\theta)}, \vec{p}, s|\mathcal{O}(x_0)|1^{(\theta)}, \vec{p}, s\rangle\langle 1^{(\theta)}, \vec{p}, s|\bar{\chi}^\beta(x_0)|0\rangle, \\ C^{(\theta)(2)\alpha\beta}(\vec{p}) &= N^2\langle 0|\chi^\alpha(x_0)|1^{(\theta)}, \vec{p}, s\rangle\langle 1^{(\theta)}, \vec{p}, s|\mathcal{O}(x_0)|0^{(\theta)}, \vec{p}, s\rangle\langle 0^{(\theta)}, \vec{p}, s|\bar{\chi}^\beta(x_0)|0\rangle, \\ f^{(1)\alpha\beta}(n_1^{(\theta)}, n_2^{(\theta')}, \vec{p}) &= N^2 \sum_s \langle 0|\chi^\alpha(x_0)|n_2^{(\theta')}, \vec{p}, s\rangle\langle n_2^{(\theta')}, \vec{p}, s|\mathcal{O}(x_0)|n_1^{(\theta)}, \vec{p}, s\rangle\langle n_1^{(\theta)}, \vec{p}, s|\bar{\chi}^\beta(x_0)|0\rangle. \end{aligned} \tag{A3}$$

(ii) When $t_1 > t_2 > t_0$, we get

$$G^{\alpha\beta}_{N\mathcal{O}N}(t_2, t_1, \vec{p}) = N^2 \sum_{n_1,n_2,s} e^{-E_0^{n_2}(t_1-t_2)} e^{-E_p^{n_1}(t_2-t_0)} \langle 0|\mathcal{O}(x_0)|n_2, \vec{0}, s\rangle\langle n_2, \vec{0}, s|\chi^\alpha(x_0)|n_1, \vec{p}, s\rangle\langle n_1, \vec{p}, s|\bar{\chi}^\beta(x_0)|0\rangle$$
$$= 0. \qquad [\text{since, for a twist-two operator, } \langle 0|\mathcal{O}(x_0)|n_2, \vec{0}, s\rangle = 0] \tag{A4}$$

(iii) When $t_2 > t_0 > t_1$, we get

$$G^{\alpha\beta}_{N\mathcal{O}N}(t_2, t_1, \vec{p}) = N^2 \sum_{n_1,n_2,s} e^{-E_p^{n_2}(t_2-t_0)} e^{-E_0^{n_1}(t_0-t_1)} \langle 0|\chi^\alpha(x_0)|n_2, \vec{p}, s\rangle\langle n_2, \vec{p}, s|\bar{\chi}^\beta(x_0)|n_1, \vec{0}, s\rangle\langle n_1, \vec{0}, s|\mathcal{O}(x_0)|0\rangle$$
$$= 0. \qquad [\text{since, for a twist-two operator, } \langle n_1, \vec{0}, s|\mathcal{O}(x_0)|0\rangle = 0] \tag{A5}$$

2. Ratios for disconnected insertion

We will show a sample calculation for extracting the disconnected first and second moments by considering the $\mathcal{O} = \mathcal{O}_{4i}$ operator, where $i = 1, 2, 3$. The calculation for the other operators will be similar. For this operator, we will use the nucleon with one unit of lattice momentum in the i-th direction. First consider the first and the second terms of Eq. (A2) only. Taking the trace with parity projection operator, $\Gamma^{\beta\alpha}$ in Eq. (A2), we get

$$\begin{aligned}
&\Gamma^{\beta\alpha} \times [\text{first term} + \text{second term of Eq. (A2)}] \\
&= N^2 \sum_s e^{-E_p^{0+}(t_2-t_0)} \frac{a^3}{(2\kappa)^{3/2}} \left(\frac{m^+}{NE_p^{0+}}\right)^{1/2} \phi^+ \frac{a^3}{(2\kappa)^{3/2}} \left(\frac{m^+}{NE_p^{0+}}\right)^{1/2} \phi^{+*} \bar{u}^{+\beta}(\vec{p}, s) \Gamma^{\beta\alpha} u^{+\alpha}(\vec{p}, s) \frac{m^+}{\kappa N E_p^{0+}} \frac{\langle x\rangle(-ip_4)p_i}{2m^+} \\
&\quad + N^2 \sum_s e^{-E_p^{0-}(t_2-t_0)} \frac{a^3}{(2\kappa)^{3/2}} \left(\frac{m^-}{NE_p^{0-}}\right)^{1/2} \phi^- \frac{a^3}{(2\kappa)^{3/2}} \left(\frac{m^-}{NE_p^{0-}}\right)^{1/2} \phi^{-*} (\bar{u}^{-\beta}(\vec{p}, s)\gamma_5) \Gamma^{\beta\alpha} (\gamma_5 u^{-\alpha}(\vec{p}, s)) \frac{m^-}{\kappa N E_p^{0-}} \frac{\langle x\rangle^-(-ip_4)p_i}{2m^-} \\
&= \frac{a^6}{(2\kappa)^3} \frac{m^+}{E_p^{0+}} |\phi^+|^2 e^{-E_p^{0+}(t_2-t_0)} \left(1 + \frac{m^-}{E_p^{0-}} \frac{E_p^{0+}}{m^+}\right) \frac{\langle x\rangle p_i}{2\kappa},
\end{aligned} \tag{A6}$$

where $\langle x\rangle^+ = \langle x\rangle$ is the first moment, $\langle x\rangle^-$ is an unknown constant.

We will now sum $\mathrm{Tr}[\Gamma G_{N\mathcal{O}N}(t_2, t_1, \vec{p})]$ over the current insertion time, t_1, from an initial time, $t_i = t_0 + 1$, to a final time, $t_f = t_2 - 1$, so that, $t_f > t_i > t_0$, where the nucleon source is at t_0, and t_2 is the sink time. Then, by using Eqs. (A2), (A3), and (A6), we get

$$\begin{aligned}
\sum_{t_1=t_i}^{t_f} \mathrm{Tr}[\Gamma G_{N\mathcal{O}_{4i}N}(t_2, t_1, p_i)] &= \sum_{t_1}^{t_f} \Gamma^{\beta\alpha} G^{\alpha\beta}_{N\mathcal{O}_{4i}N}(t_2, t_1, \vec{p}) \\
&= \sum_{t_1=t_i}^{t_f} \frac{a^6}{(2\kappa)^3} \frac{m}{E_p^{0+}} |\phi|^2 e^{-E_p^0(t_2-t_0)} \left(1 + \frac{m^-}{E_p^{0-}} \frac{E_p^{0+}}{m}\right) \frac{\langle x\rangle p_i}{2\kappa} \\
&\quad + \sum_{\theta=+,-} [e^{-E_p^{0(\theta)}(t_2-t_1)} e^{-E_p^{1(\theta)}(t_1-t_0)} \tilde{C}_{4i}^{(\theta)(1)}(\vec{p}) + e^{-E_p^{1(\theta)}(t_2-t_1)} e^{-E_p^{0(\theta)}(t_1-t_0)} \tilde{C}_{4i}^{(\theta)(2)}(\vec{p})] \\
&\quad + \sum_{\theta,\theta'=+,-} \sum_{n_1^{(\theta)}, n_2^{(\theta')}=1}^{\infty} [e^{-E_p^{n_2^{(\theta')}}(t_2-t_1)} e^{-E_p^{n_1^{(\theta)}}(t_1-t_0)} \tilde{f}_{4i}^{(1)}(n_1^{(\theta)}, n_2^{(\theta')}, \vec{p})].
\end{aligned} \tag{A7}$$

Dividing by the two-point function, we get

$$\sum_{t_1=t_i}^{t_f}\frac{\mathrm{Tr}[G_{N\mathcal{O}_{4i}N}(t_2,t_1,\vec{p})]}{\mathrm{Tr}[\Gamma G_{NN}(t_2,\vec{p})]}=\Bigg[\frac{\langle x\rangle p_i}{2\kappa}t_2-\frac{\langle x\rangle p_i}{2\kappa}t_i+\mathrm{k}_1\mathrm{k}_2-\mathrm{k}_1\mathrm{k}_5-[\mathrm{k}_1\mathrm{k}_3-\mathrm{k}_1\mathrm{k}_4]\sum_{\theta=+,-}e^{-(E_p^{1(\theta)}-E_p^{0(\theta)})(t_2-t_0)}$$
$$+\mathrm{k}_1\sum_{\theta'=+,-}\sum_{n'^{(\theta')}=1}^{\infty}e^{-(E_p^{n'(\theta')}-E_p^{0(\theta')})(t_2-t_0)}g_3(n'^{(\theta')},\vec{p})\Bigg]$$
$$+\Bigg[1+\mathrm{k}_1\sum_{m=1}^{\infty}\Bigg(-\sum_{\theta=+,-}\sum_{n^{(\theta)}=1}^{\infty}e^{-(E_p^{n(\theta)}-E_p^{0})(t_2-t_0)}\tilde{f}(n^{(\theta)},\vec{p})\Bigg)^m\Bigg], \tag{A8}$$

where

$$\tilde{f}(n^{+,-},\vec{p})=N\Gamma^{\alpha\beta}\sum_s\langle 0|\chi^\alpha(x_0)|n^{+,-},\vec{p},s\rangle\times\langle n^{+,-},\vec{p},s|\bar{\chi}^\beta(x_0)|0\rangle,$$
$$\mathrm{k}_1=\frac{a^6}{(2\kappa)^3}\frac{m}{E_p^0}|\phi|^2\Bigg(1+\frac{m^-}{E_p^{0-}}\frac{E_p^0}{m}\Bigg)(=\text{constant}),$$
$$\mathrm{k}_2=\sum_{\theta=+,-}\frac{e^{-(E_p^{1(\theta)}-E_p^{0(\theta)})(t_i-t_0)}}{1-e^{-(E_p^{1(\theta)}-E_p^{0(\theta)})}}\tilde{C}_{4i}^{(\theta)(1)}(=\text{constant}),$$
$$\mathrm{k}_3=\sum_{\theta=+,-}\frac{1}{1-e^{-(E_p^{1(\theta)}-E_p^{0(\theta)})}}\tilde{C}_{4i}^{(\theta)(1)}(=\text{constant}),$$
$$\mathrm{k}_4=\sum_{\theta=+,-}\frac{e^{(E_p^{1(\theta)}-E_p^{0(\theta)})(t_i-t_0)}}{1-e^{(E_p^{1(\theta)}-E_p^{0(\theta)})}}\tilde{C}_{4i}^{(\theta)(2)}(=\text{constant}),$$
$$\mathrm{k}_5=\sum_{\theta=+,-}\frac{1}{1-e^{(E_p^{1(\theta)}-E_p^{0(\theta)})}}\tilde{C}_{4i}^{(\theta)(2)}(=\text{constant}),$$
$$g_3(n^{(\theta)},\vec{p})=\sum_{\theta=+,-}\sum_{n_1^{(\theta')}=1}^{\infty}\Bigg[e^{-(E_p^{n^{(\theta)}}-E_p^{n_1^{(\theta')}})(t_0-t_i)}\times\frac{\tilde{f}_{4i}^{(1)}(n_1^{(\theta')},n^{(\theta)},\vec{p})}{1-e^{(E_p^{n^{(\theta)}}-E_p^{n_1^{(\theta')}})}}-\frac{\tilde{f}_{4i}^{(1)}(n^{(\theta)},n_1^{(\theta')},\vec{p})}{1-e^{(E_p^{n_1^{(\theta')}}-E_p^{n^{(\theta)}})}}\Bigg]. \tag{A9}$$

From Eq. (A8), we get

$$\sum_{t_1=t_i}^{t_f}\frac{\mathrm{Tr}[G_{N\mathcal{O}_{4i}N}(t_2,t_1,\vec{p})]}{\mathrm{Tr}[\Gamma G_{NN}(t_2,\vec{p})]}\xrightarrow{(t_2-t_0)\gg 1}\frac{\langle x\rangle p_i}{2\kappa}t_2+\text{const}, \tag{A10}$$

where

$$\text{const}=-\frac{\langle x\rangle p_i}{2\kappa}t_i+\mathrm{k}_1\mathrm{k}_2-\mathrm{k}_1\mathrm{k}_5. \tag{A11}$$

APPENDIX B: UNBIASED SUBTRACTION

The set of traceless matrices is obtained from the hopping parameter expansion of the inverse of the fermion matrix M which is given by

$$S=M^{-1}=I+\kappa D+\kappa^2D^2+\kappa^3D^3+\cdots, \tag{B1}$$

where

$$D_{x,y}=\sum_{\mu=1}^{4}[(1-\gamma_\mu)_{\alpha\beta}U_\mu^{ab}(x)\delta_{x,y-a_\mu}+(1+\gamma_\mu)_{\alpha\beta}U_\mu^{\dagger ab}(x-a_\mu)\delta_{x,y+a_\mu}], \tag{B2}$$

x, y are space-time coordinates, α, β are spin indices, and a, b are color indices. If for some currents, some powers of D are not traceless, we make them traceless by subtracting their traces from themselves. Now, we are going to calculate the traces for all the three currents. We suppress the argument U from each of the propagators for convenience.

1. Two-index operators

The disconnected part of $\mathcal{O}_{\mu\nu}$ is given by

$$\text{Loop}=\frac{\lambda}{8a}\sum_{\vec{x}_1}[\mathrm{Tr}[S^{(f)mn}(x_1+a_\nu,x_1)\gamma_\mu U_\nu^{nm}(x_1)]-\mathrm{Tr}[S^{(f)mn}(x_1-a_\nu,x_1)\gamma_\mu U_\nu^{\dagger nm}(x_1-a_\nu)]+\mathrm{Tr}[S^{(f)mn}(x_1,x_1-a_\nu)\gamma_\mu U_\nu^{nm}(x_1-a_\nu)]-\mathrm{Tr}[S^{(f)mn}(x_1,x_1+a_\nu)\gamma_\mu U_\nu^{\dagger nm}(x_1)]+\mu\leftrightarrow\nu], \tag{B3}$$

where $\lambda=-i$ for $\mu=4$, $\nu=1,2,3$; $\lambda=+1$ for $\mu=\nu=1,2,3$ and $\lambda=-1$ for $\mu=\nu=4$. Let us consider the first term of the loop

$$\frac{\lambda}{8a}\sum_{\vec{x}_1}\mathrm{Tr}[S^{(f)mn}(x_1+a_\nu,x_1)\gamma_\mu U_\nu^{nm}(x_1)]$$
$$\simeq\frac{\lambda}{8a}\sum_{\vec{x}_1}\sum_{m,\xi}\langle\eta^\dagger_{x_1,n,\tau}X_{x_1+a_\nu,m,\xi}\rangle(\gamma_\mu)_{\tau\xi}U_\nu^{nm}(x_1)[\text{using noise}]$$
$$=\frac{\lambda}{8a}\sum_{\vec{x}_1}\sum_{m,\xi,k,\sigma}\frac{1}{L}\sum_{l=1}^{L}\eta^{l\dagger}_{x_1,n,\tau}M^{(-1)mk}_{\xi\sigma}(x_1+a_\nu,z)\times\eta^l_{z,k,\sigma}(\gamma_\mu)_{\tau\xi}U_\nu^{nm}(x_1). \tag{B4}$$

In Eq. (B4), we will substitute the hopping parameter expansion of M^{-1}. Then, from Eq. (B4), the term becomes

$$\sum_{\vec{x}_1}\mathrm{Tr}[S^{(f)mn}(x_1+a_\nu,x_1)\gamma_\mu U_\nu^{nm}(x_1)]$$

$$\approx \sum_{\vec{x}_1}\sum_{m,\xi}\frac{1}{L}\sum_{l=1}^{L}\eta^{l\dagger}_{x_1,n,\tau}\eta^{l}_{x_1+a_\nu,m,\xi}(\gamma_\mu)_{\tau\xi}U_\nu^{nm}(x_1). \quad \text{(B5)}$$

Similarly, if we consider the fourth term of the Loop in Eq. (B3), we get

$$\frac{\lambda}{8a}\sum_{\vec{x}_1}\mathrm{Tr}[S^{(f)mn}(x_1,x_1+a_\nu)\gamma_\mu U_\nu^{\dagger nm}(x_1)]$$

$$\approx \frac{\lambda}{8a}\sum_{\vec{x}_1}\sum_{m,\xi}\frac{1}{L}\sum_{l=1}^{L}\eta^{l\dagger}_{x_1+a_\nu,n,\tau}\eta^{l}_{x_1,m,\xi}(\gamma_\mu)_{\tau\xi}U_\nu^{\dagger nm}(x_1). \quad \text{(B6)}$$

Combining Eqs. (B5) and (B6), we find that

$$\frac{\lambda}{8a}[\mathrm{Tr}[S^{(f)mn}(x_1+a_\nu,x_1)\gamma_\mu U_\nu^{nm}(x_1)] - \mathrm{Tr}[S^{(f)mn}(x_1,x_1+a_\nu)\gamma_\mu U_\nu^{\dagger nm}(x_1)]]$$

$$=\frac{\lambda}{8a}\sum_{\vec{x}_1}\sum_{m,\xi}\frac{1}{L}\sum_{l=1}^{L}2\,\mathrm{Im}[\eta^{l\dagger}_{x_1,n,\tau}\eta^{l}_{x_1+a_\nu,m,\xi}(\gamma_\mu)_{\tau\xi}U_\nu^{nm}(x_1)]. \quad \text{(B7)}$$

By considering similar combinations of other terms, we can prove that for the $\mathcal{O}_{\mu\mu}$ operator, the real part of the loop is zero for the first term, I, and for the $\mathcal{O}_{4i}$ operator, the imaginary part is zero. So, we cannot consider the first term, I. If we substitute M^{-1} by κ^2D^2 and κ^4D^4, the trace is going to be zero, since there will be no plaquette term. But if we substitute M^{-1} by κD and κ^3D^3, there is a possibility of having a nonzero trace. Since the operators, $\mathcal{O}_{4i}$ and $\mathcal{O}_{\mu\mu}$, can have different traces (or, no traces), we will consider them separately.

(i) *First term of* $\mathcal{O}_{4i}$:

$$\frac{-i}{8a}\sum_{\vec{x}_1}\mathrm{Tr}[S^{(f)mn}(x_1+a_i,x_1)\gamma_4 U_i^{nm}(x_1)]$$

$$\simeq\frac{-i}{8a}\sum_{\vec{x}_1}\sum_{m,\xi,k,\sigma}\frac{1}{L}\sum_{l=1}^{L}\eta^{l\dagger}_{x_1,n,\tau}M^{(-1)mk}_{\xi\sigma}(x_1+a_i,z)\times\eta^{l}_{z,k,\sigma}(\gamma_4)_{\tau\xi}U_i^{nm}(x_1). \quad \text{(B8)}$$

If we substitute $M^{-1}(x_1+a_i,z)$ in Eq. (B8) by κD, the only nonvanishing term could be,

$$\sum_{\mu=1}^{4}(1+\gamma_\mu)_{\alpha\beta}U_\mu^{\dagger ab}(x-a_\mu)\delta_{x,y+a_\mu}.$$

So we get

$$\frac{-i}{8a}\sum_{\vec{x}_1}\mathrm{Tr}[S^{(f)mn}(x_1+a_i,x_1)\gamma_4 U_i^{nm}(x_1)]$$

$$\simeq\frac{-i}{8a}\kappa\sum_{\vec{x}_1}\sum_{m,\xi,k,\sigma}\frac{1}{L}\sum_{l=1}^{L}\eta^{l\dagger}_{x_1,n,\tau}\Big[\sum_{\mu=1}^{4}(1+\gamma_\mu)_{\xi\sigma}U_\mu^{\dagger mk}(x_1+a_i-a_\mu)\delta_{x_1+a_i,z+a_\mu}\Big]\times\eta^{l}_{z,k,\sigma}(\gamma_4)_{\tau\xi}U_i^{nm}(x_1)$$

$$=\frac{-i}{8a}\kappa\sum_{\vec{x}_1}\sum_{m,\xi,k,\sigma}\delta_{(n,k)(\tau,\sigma)}(\gamma_4)_{\tau\xi}(1+\gamma_i)_{\xi\sigma}U_i^{\dagger mk}(x_1)U_i^{nm}(x_1)\quad(\text{putting }\mu=i)=0. \quad \text{(B9)}$$

We now replace $M^{(-1)}$ by κ^3D^3, the nonvanishing terms could be

$$\sum_{\mu',\nu',\rho}[\{(1-\gamma_{\mu'})(1+\gamma_{\nu'})(1+\gamma_\rho)\}_{\alpha\beta}\{U_{\mu'}(x)U^\dagger_{\nu'}(x+a_{\mu'}-a_{\nu'})U^\dagger_\rho(x+a_{\mu'}-a_{\nu'}-a_\rho)\}^{ab}\delta_{x+a_{\mu'}-a_{\nu'},y+a_\rho}$$
$$+\{(1+\gamma_{\mu'})(1-\gamma_{\nu'})(1+\gamma_\rho)\}_{\alpha\beta}\{U^\dagger_{\mu'}(x-a_{\mu'})U_{\nu'}(x-a_{\mu'})U^\dagger_\rho(x-a_{\mu'}+a_{\nu'}-a_\rho)\}^{ab}\delta_{x-a_{\mu'}+a_{\nu'},y+a_\rho}$$
$$+\{(1+\gamma_{\mu'})(1+\gamma_{\nu'})(1-\gamma_\rho)\}_{\alpha\beta}\{U^\dagger_{\mu'}(x-a_{\mu'})U^\dagger_{\nu'}(x-a_{\mu'}-a_{\nu'})U_\rho(x-a_{\mu'}-a_{\nu'})\}^{ab}\delta_{x-a_{\mu'}-a_{\nu'},y-a_\rho}]. \quad \text{(B10)}$$

Let us consider the first term of Eq. (B10).

$$\frac{-i}{8a}\sum_{\vec{x}_1}\mathrm{Tr}[S^{(f)mn}(x_1+a_i,x_1)\gamma_4 U_i^{nm}(x_1)]$$
$$=\frac{-i}{8a}\kappa^3\sum_{\vec{x}_1}\sum_{m,\xi,k,\sigma}\frac{1}{L}\sum_{l=1}^{L}\eta^{l\dagger}_{x_1,n,\tau}\sum_{\mu',\nu',\rho}[\{(1-\gamma_{\mu'})(1+\gamma_{\nu'})(1+\gamma_\rho)\}_{\xi\sigma}\{U_{\mu'}(x_1+a_i)U^\dagger_{\nu'}(x_1+a_i+a_{\mu'}-a_{\nu'})$$
$$\times U^\dagger_\rho(x_1+a_i+a_{\mu'}-a_{\nu'}-a_\rho)\}^{mk}\delta_{x_1+a_i+a_{\mu'}-a_{\nu'},z+a_\rho}]\eta^l_{z,k,\sigma}(\gamma_4)_{\tau\xi}U_i^{nm}(x_1). \tag{B11}$$

In order to have nonvanishing delta function, we must have either $\mu'=\rho$, $\nu'=i$; or $\mu'=\nu'$, $\rho=i$; or $\mu'=\rho=\nu'=i$. Let us take the case $\mu'=\rho$, $\nu'=i$. Then the first term of Eq. (B10) gives

$$\frac{-i}{8a}\kappa^3\sum_{\vec{x}_1}\sum_{m,\xi,k,\sigma}\sum_{\mu'}\delta_{(n,k)(\tau,\sigma)}(\gamma_4)_{\tau\xi}(1-\gamma_{\mu'})(1+\gamma_i)(1+\gamma_{\mu'})_{\xi\sigma}\{U_{\mu'}(x_1+a_i)U_i^\dagger(x_1+a_{\mu'})U^\dagger_{\mu'}(x_1)\}^{mk}U_i^{nm}(x_1)$$
$$=\frac{-i}{8a}\kappa^3\sum_{\vec{x}_1}\sum_{m,\xi}\sum_{\mu'}\{(\gamma_4-\gamma_4\gamma_{\mu'})(1+\gamma_i)(1+\gamma_{\mu'})_{\xi\xi}\{U_{\mu'}(x_1+a_i)U_i^\dagger(x_1+a_{\mu'})U^\dagger_{\mu'}(x_1)U_i(x_1)\}^{mm}=0. \tag{B12}$$

For other two possibilities $\mu'=\nu'$, $\rho=i$ and $\mu'=\rho=\nu'=i$, the trace for the spin part is zero due to the multiplication of γ matrices.

It can be shown that second and third terms of Eq. (B10) also have zero traces. In a similar manner, we can show that other terms of the operator $\mathcal{O}_{4i}$ also have zero trace.

Now, we will consider the operator, $\mathcal{O}_{\mu\mu}$.

(ii) *First term of* $\mathcal{O}_{\mu\mu}$:

$$\frac{\lambda}{8a}\sum_{\vec{x}_1}\mathrm{Tr}[S^{(f)mn}(x_1+a_\mu,x_1)\gamma_\mu U_\mu^{nm}(x_1)]\simeq\frac{\lambda}{8a}\sum_{\vec{x}_1}\sum_{m,\xi,k,\sigma}\frac{1}{L}\sum_{l=1}^{L}\eta^{l\dagger}_{x_1,n,\tau}M^{(-1)mk}_{\xi\sigma}(x_1+a_\mu,z)\eta^l_{z,k,\sigma}(\gamma_\mu)_{\tau\xi}U_\mu^{nm}(x_1), \tag{B13}$$

where $\lambda=+1$ for $\mu=\nu=1,2,3$ and $\lambda=-1$ for $\mu=\nu=4$.

If we substitute $M^{-1}(x_1+a_\mu,z)$ in Eq. (B13) by κD, the only nonvanishing term could be

$$\sum_{\nu=1}^{4}(1+\gamma_\nu)_{\alpha\beta}U_\nu^{\dagger ab}(x-a_\nu)\delta_{x,y+a_\nu}.$$

So we get

$$\frac{\lambda}{8a}\sum_{\vec{x}_1}\mathrm{Tr}[S^{(f)mn}(x_1+a_\mu,x_1)\gamma_\mu U_\mu^{nm}(x_1)]$$
$$\simeq\frac{\lambda}{8a}\kappa\sum_{\vec{x}_1}\sum_{m,\xi,k,\sigma}\frac{1}{L}\sum_{l=1}^{L}\eta^{l\dagger}_{x_1,n,\tau}\Big[\sum_{\nu=1}^{4}(1+\gamma_\nu)_{\xi\sigma}U_\nu^{\dagger mk}(x_1+a_\mu-a_\nu)\delta_{x_1+a_\mu,z+a_\nu}\Big]$$
$$\times\eta^l_{z,k,\sigma}(\gamma_\mu)_{\tau\xi}U_\mu^{nm}(x_1)$$
$$=\frac{\lambda}{8a}\kappa\sum_{\vec{x}_1}\sum_{m,\xi,k,\sigma}\delta_{(n,k)(\tau\sigma)}(\gamma_\mu)_{\tau\xi}(1+\gamma_\mu)_{\xi\sigma}U_\mu^{\dagger mk}(x_1)U_\mu^{nm}(x_1)\qquad(\text{putting }\nu=\mu)=\frac{\lambda}{8a}12\kappa V^3. \tag{B14}$$

And, if we substitute $M^{-1}(x_1+a_\mu,z)$ by κ^3D^3, the nonvanishing terms could be

$$\kappa^3 \sum_{\mu',\nu',\rho} [\{(1-\gamma_{\mu'})(1+\gamma_{\nu'})(1+\gamma_\rho)\}_{\alpha\beta}\{U_{\mu'}(x)U^\dagger_{\nu'}(x+a_{\mu'}-a_{\nu'})U^\dagger_\rho(x+a_{\mu'}-a_{\nu'}-a_\rho)\}^{ab}\delta_{x+a_{\mu'}-a_{\nu'},y+a_\rho}$$
$$+\{(1+\gamma_{\mu'})(1-\gamma_{\nu'})(1+\gamma_\rho)\}_{\alpha\beta}\{U^\dagger_{\mu'}(x-a_{\mu'})U_{\nu'}(x-a_{\mu'})U^\dagger_\rho(x-a_{\mu'}+a_{\nu'}-a_\rho)\}^{ab}\delta_{x-a_{\mu'}+a_{\nu'},y+a_\rho}$$
$$+\{(1+\gamma_{\mu'})(1+\gamma_{\nu'})(1-\gamma_\rho)\}_{\alpha\beta}\{U^\dagger_{\mu'}(x-a_{\mu'})U^\dagger_{\nu'}(x-a_{\mu'}-a_{\nu'})U_\rho(x-a_{\mu'}-a_{\nu'})\}^{ab}\delta_{x-a_{\mu'}-a_{\nu'},y-a_\rho}]. \tag{B15}$$

Let us consider the first term of Eq. (B15)

$$\frac{\lambda}{8a}\sum_{\vec{x}_1}\mathrm{Tr}[S^{(f)mn}(x_1+a_\mu,x_1)\gamma_\mu U^{nm}_\mu(x_1)]$$
$$\simeq \frac{\lambda}{8a}\kappa^3\sum_{\vec{x}_1}\sum_{m,\xi,k,\sigma}\frac{1}{L}\sum_{l=1}^{L}\eta^{l\dagger}_{x_1,n,\tau}\sum_{\mu',\nu',\rho}[\{(1-\gamma_{\mu'})(1+\gamma_{\nu'})(1+\gamma_\rho)\}_{\xi\sigma}\{U_{\mu'}(x_1+a_\mu)U^\dagger_{\nu'}(x_1+a_\mu+a_{\mu'}-a_{\nu'})$$
$$\times U^\dagger_\rho(x_1+a_\mu+a_{\mu'}-a_{\nu'}-a_\rho)\}^{mk}\delta_{x_1+a_\mu+a_{\mu'}-a_{\nu'},z+a_\rho}]\eta^l_{z,k,\sigma}(\gamma_\mu)_{\tau\xi}U^{nm}_\mu(x_1). \tag{B16}$$

In order to have nonvanishing delta function, we must have either $\mu'=\rho$, $\nu'=\mu$, or $\mu'=\nu'$, $\rho=\mu$, or $\mu'=\rho=\nu'=\mu$. Let us take the case $\mu'=\rho$, $\nu'=\mu$. Then the first term of Eq. (B15) gives

$$\frac{\lambda}{8a}\kappa^3\sum_{\vec{x}_1}\sum_{m,\xi,k,\sigma}\sum_{\mu'}\delta_{(n,k)(\tau,\sigma)}(\gamma_\mu)_{\tau\xi}(1-\gamma_{\mu'})(1+\gamma_\mu)(1+\gamma_{\mu'})_{\xi\sigma}\{U_{\mu'}(x_1+a_\mu)U^\dagger_\mu(x_1+a_{\mu'})U^\dagger_{\mu'}(x_1)\}^{mk}U^{nm}_\mu(x_1)$$
$$=8\frac{\lambda}{8a}\kappa^3\sum_{\vec{x}_1}\sum_{m}\sum_{\mu'\neq\mu}\{U_{\mu'}(x_1+a_\mu)U^\dagger_\mu(x_1+a_{\mu'})U^\dagger_{\mu'}(x_1)U_\mu(x_1)\}^{mm}. \tag{B17}$$

For other two possibilities $\mu'=\nu'$, $\rho=\mu$ and $\mu'=\rho=\nu'=\mu$, the trace for the spin part is zero due to the multiplication of γ matrices. Let now us consider the second term of Eq. (B15). Then

$$\frac{\lambda}{8a}\sum_{\vec{x}_1}\mathrm{Tr}[S^{(f)mn}(x_1+a_\mu,x_1)\gamma_\mu U^{nm}_\mu(x_1)]$$
$$\simeq \frac{\lambda}{8a}\kappa^3\sum_{\vec{x}_1}\sum_{m,\xi,k,\sigma}\frac{1}{L}\sum_{l=1}^{L}\eta^{l\dagger}_{x_1,n,\tau}\sum_{\mu',\nu',\rho}[\{(1+\gamma_{\mu'})(1-\gamma_{\nu'})(1+\gamma_\rho)\}_{\xi\sigma}\{U^\dagger_{\mu'}(x_1+a_\mu-a_{\mu'})U_{\nu'}(x_1+a_\mu-a_{\mu'})$$
$$\times U^\dagger_\rho(x_1+a_\mu-a_{\mu'}+a_{\nu'}-a_\rho)\}^{mk}\delta_{x_1+a_\mu-a_{\mu'}+a_{\nu'},z+a_\rho}]\eta^l_{z,k,\sigma}(\gamma_\mu)_{\tau\xi}U^{nm}_\mu(x_1). \tag{B18}$$

In order to have nonvanishing delta function, we must have either $\mu'=\mu$, $\rho=\nu'$, or $\mu'=\nu'$, $\rho=\mu$, or $\mu'=\rho=\nu'=\mu$. Let us take the case $\mu'=\mu$, $\nu'=\rho$. Then the second term of Eq. (B15) gives

$$\frac{\lambda}{8a}\kappa^3\sum_{\vec{x}_1}\sum_{m,\xi,k,\sigma}\sum_{\mu'}\delta_{(n,k)(\tau,\sigma)}(\gamma_\mu)_{\tau\xi}\{(1+\gamma_\mu)(1-\gamma_{\nu'})(1+\gamma_{\nu'})\}_{\xi\sigma}\{U^\dagger_\mu(x_1)U_{\nu'}(x_1)U^\dagger_{\nu'}(x_1)\}^{mk}U^{nm}_\mu(x_1)=0. \tag{B19}$$

For other two possibilities $\mu'=\nu'$, $\rho=\mu$, and $\mu'=\rho=\nu'=\mu$, the traces for the spin part are zero due to the multiplication of γ matrices. Let us consider the third term of Eq. (B15). Then

$$\frac{\lambda}{8a}\sum_{\vec{x}_1}\mathrm{Tr}[S^{(f)mn}(x_1+a_\mu,x_1)\gamma_\mu U^{nm}_\mu(x_1)]$$
$$=\frac{\lambda}{8a}\kappa^3\sum_{\vec{x}_1}\sum_{m,\xi,k,\sigma}\frac{1}{L}\sum_{l=1}^{L}\eta^{l\dagger}_{x_1,n,\tau}\sum_{\mu',\nu',\rho}[\{(1+\gamma_{\mu'})(1+\gamma_{\nu'})(1-\gamma_\rho)\}_{\xi\sigma}\{U^\dagger_{\mu'}(x_1+a_\mu-a_{\mu'})U^\dagger_{\nu'}(x_1+a_\mu-a_{\mu'}-a_{\nu'})$$
$$\times U_\rho(x_1+a_\mu-a_{\mu'}-a_{\nu'})\}^{mk}\delta_{x_1+a_\mu-a_{\mu'}-a_{\nu'},z-a_\rho}]\eta^l_{z,k,\sigma}(\gamma_\mu)_{\tau\xi}U^{nm}_\mu(x_1). \tag{B20}$$

In order to have nonvanishing delta function, we must have either $\mu'=\rho$, $\nu'=\mu$, or $\mu'=\mu$, $\rho=\nu'$, or $\mu'=\rho=\nu'=\mu$. Let us take the case $\mu'=\rho$, $\nu'=\mu$. Then the third term of Eq. (B15) gives

$$\frac{\lambda}{8a}\kappa^3\sum_{\vec{x}_1}\sum_{m,\xi,k,\sigma}\sum_{\mu'}\delta_{(n,k)(\tau,\sigma)}(\gamma_\mu)_{\tau\xi}(1+\gamma_{\mu'})(1+\gamma_\mu)(1-\gamma_{\mu'})_{\xi\sigma}\{U^\dagger_{\mu'}(x_1+a_\mu-a_{\mu'})U^\dagger_\mu(x_1-a_{\mu'})$$
$$\times U_{\mu'}(x_1-a_{\mu'})\}^{mk}U^{nm}_\mu(x_1)$$
$$=\frac{\lambda}{8a}8\kappa^3\sum_{\vec{x}_1}\sum_m\sum_{\mu'\neq\mu}\{U^\dagger_{\mu'}(x_1+a_\mu-a_{\mu'})U^\dagger_\mu(x_1-a_{\mu'})U_{\mu'}(x_1-a_{\mu'})U_\mu(x_1)\}^{mm}. \tag{B21}$$

For other two possibilities $\mu'=\mu$, $\rho=\nu'$, and $\mu'=\rho=\nu'=\mu$, the traces for the spin part are zero due to the multiplication of γ matrices.

Doing similar calculations for other terms of $\mathcal{O}_{\mu\mu}$, we get the trace for the κD term

$$\text{Trace}=\frac{\lambda}{8a}2\kappa[12V^3-(-12V^3)+12V^3-(-12V^3)]=\frac{\lambda}{8a}96\kappa V^3, \tag{B22}$$

and for the κ^3D^3 term

$$\begin{aligned}\text{Trace}\simeq\frac{\lambda}{8a}16\kappa^3&\sum_{\vec{x}_1}\sum_m\sum_{\mu'\neq\mu}[[\{U_{\mu'}(x_1+a_\mu)U^\dagger_\mu(x_1+a_{\mu'})U^\dagger_{\mu'}(x_1)U_\mu(x_1)+U^\dagger_{\mu'}(x_1+a_\mu-a_{\mu'})U^\dagger_\mu(x_1-a_{\mu'})\\
&\times U_{\mu'}(x_1-a_{\mu'})U_\mu(x_1)\}^{mm}]-[-\{U_{\mu'}(x_1-a_\mu)U_\mu(x_1-a_\mu+a_{\mu'})U^\dagger_{\mu'}(x_1)U^\dagger_\mu(x_1-a_\mu)\\
&+U^\dagger_{\mu'}(x_1-a_\mu-a_{\mu'})U_\mu(x_1-a_\mu-a_{\mu'})U_{\mu'}(x_1-a_{\mu'})U^\dagger_\mu(x_1-a_\mu)\}^{mm}]\\
&+[\{U_{\mu'}(x_1-a_\mu)U_\mu(x_1-a_\mu+a_{\mu'})U^\dagger_{\mu'}(x_1)U^\dagger_\mu(x_1-a_\mu)+U^\dagger_{\mu'}(x_1-a_\mu-a_{\mu'})U_\mu(x_1-a_\mu-a_{\mu'})\\
&\times U_{\mu'}(x_1-a_{\mu'})U^\dagger_\mu(x_1-a_\mu)\}^{mm}]^\dagger-[-\{U_{\mu'}(x_1+a_\mu)U^\dagger_\mu(x_1+a_{\mu'})U^\dagger_{\mu'}(x_1)U_\mu(x_1)\\
&+U^\dagger_{\mu'}(x_1+a_\mu-a_{\mu'})U^\dagger_\mu(x_1-a_{\mu'})U_{\mu'}(x_1-a_{\mu'})U_\mu(x_1)\}^{mm}]^\dagger]\\
=\frac{\lambda}{8a}32\kappa^3&\sum_{\vec{x}_1}\sum_m\sum_{\mu'\neq\mu}\text{Re}[\{U_{\mu'}(x_1+a_\mu)U^\dagger_\mu(x_1+a_{\mu'})U^\dagger_{\mu'}(x_1)U_\mu(x_1)+U_\mu(x_1)U^\dagger_{\mu'}(x_1+a_\mu-a_{\mu'})\\
&\times U^\dagger_\mu(x_1-a_{\mu'})U_{\mu'}(x_1-a_{\mu'})+U_\mu(x_1-a_\mu+a_{\mu'})U^\dagger_{\mu'}(x_1)U^\dagger_\mu(x_1-a_\mu)U_{\mu'}(x_1-a_\mu)\\
&+U_{\mu'}(x_1-a_{\mu'})U^\dagger_\mu(x_1-a_\mu)U^\dagger_{\mu'}(x_1-a_\mu-a_{\mu'})U_\mu(x_1-a_\mu-a_{\mu'})\}^{mm}].\end{aligned} \tag{B23}$$

2. Three-index operators

As in the case of two-index operator, we can show that the first term I of the hopping expansion for this operator is real. But the loop part is imaginary. So, we can not consider the first term. If we substitute M^{-1} by κD and κ^3D^3, the trace is going to be zero, since there will be no plaquette terms. But if we substitute M^{-1} by κ^2D^2, there is a possibility of nonzero trace. One of the terms in the loop part of $\mathcal{O}_{4ii}$ is

$$\begin{aligned}&\frac{-1}{24a^2}\text{Tr}[S^{(f)mn}(x_1+a_4+a_i,x_1)(\gamma_i)\{U^{nm'}_4(x_1)U^{m'm}_i(x_1+a_4)+U^{nm'}_i(x_1)\\
&\quad\times U^{m'm}_4(x_1+a_i)\}]\\
&\simeq\frac{-1}{24a^2}\sum_{\vec{x}_1}\sum_{m,\xi,k,\sigma}\frac{1}{L}\sum_{l=1}^{L}\eta^{l\dagger}_{x_1,n,\tau}M^{(-1)mk}_{\xi\sigma}(x_1+a_4+a_i,z)\eta^l_{z,k,\sigma}(\gamma_i)_{\tau\xi}\\
&\quad\times(U^{nm'}_4(x_1)U^{m'm}_i(x_1+a_4)+U^{nm'}_i(x_1)U^{m'm}_4(x_1+a_i)).\end{aligned} \tag{B24}$$

If we substitute $M^{(-1)mk}_{\xi\sigma}$ by κ^2D^2 term, the only nonvanishing term could be

$$\sum_{\mu'=1}^{4}\sum_{\nu'=1}^{4}[\{(1+\gamma_{\mu'})(1+\gamma_{\nu'})\}_{\alpha\beta}\{U^\dagger_{\mu'}(x-a_{\mu'})U^\dagger_{\nu'}(x-a_{\mu'}-a_{\nu'})\}^{ab}\delta_{x-a_{\mu'},y+a_{\nu'}}].$$

Therefore, we get

$$
\begin{aligned}
&\frac{-1}{24a^2}\sum_{\vec{x}_1}\mathrm{Tr}[S^{(f)mn}(x_1+a_4+a_i,x_1)(\gamma_i)(U_4^{nm'}(x_1)U_i^{m'm}(x_1+a_4)\\
&\quad+U_i^{nm'}(x_1)U_4^{m'm}(x_1+a_i))]\\
&\simeq\frac{-1}{24a^2}\kappa^2\sum_{\vec{x}_1}\sum_{m,\xi,k,\sigma}\frac{1}{L}\sum_{l=1}^{L}\eta^{l\dagger}_{x_1,n,\tau}\sum_{\mu'=1,\nu'=1}^{4}[\{(1+\gamma_{\mu'})(1+\gamma_{\nu'})\}_{\xi\sigma}\\
&\quad\times\{U^\dagger_{\mu'}(x_1+a_4+a_i-a_{\mu'})U^\dagger_{\nu'}(x_1+a_4+a_i-a_{\mu'}-a_{\nu'})\}^{mk}\delta_{x_1+a_4+a_i-a_{\mu'},z+a_{\nu'}}]\\
&\quad\times\eta^{l}_{z,k,\sigma}(\gamma_i)_{\tau\xi}(U_4^{nm'}(x_1)U_i^{m'm}(x_1+a_4)+U_i^{nm'}(x_1)U_4^{m'm}(x_1+a_i))\\
&=\frac{-1}{24a^2}\kappa^2\sum_{\vec{x}_1}\sum_{m,\xi,k,\sigma}\delta_{(n,k)(\tau,\sigma)}(\gamma_i)_{\tau\xi}\{(1+\gamma_i)(1+\gamma_4)\}_{\xi\sigma}\{U_i^\dagger(x_1+a_4)U_4^\dagger(x_1)\}^{mk}[\{U_4(x_1)U_i(x_1+a_4)\}^{nm}\\
&\quad+\{U_i(x_1)U_4(x_1+a_i)\}^{nm}]\\
&\text{(putting }\mu'=i\quad\text{and}\quad\nu'=4)+\kappa^2\sum_{\vec{x}_1}\sum_{m,\xi,k,\sigma}\delta_{(n,k)(\tau,\sigma)}(\gamma_i)_{\tau\xi}\{(1+\gamma_4)(1+\gamma_i)\}_{\xi\sigma}\{U_4^\dagger(x_1+a_i)U_i^\dagger(x_1)\}^{mk}\\
&\quad\times[\{U_4(x_1)U_i(x_1+a_4)\}^{nm}+\{U_i(x_1)U_4(x_1+a_i)\}^{nm}]\quad\text{(putting }\mu'=4\quad\text{and}\quad\nu'=i)\\
&=8\frac{-1}{24a^2}\kappa^2\sum_{\vec{x}_1}\Big[\sum_m\mathrm{Re}\{U_i^\dagger(x_1+a_4)U_4^\dagger(x_1)U_i(x_1)U_4(x_1+a_i)\}^{mm}+3\Big].
\end{aligned}
\tag{B25}
$$

Calculating all the other terms in a similar manner, we can show that

$$
\begin{aligned}
\mathrm{Trace}=&\frac{-1}{24a^2}8\kappa^2\sum_{\vec{x}_1}\Big[\sum_m\mathrm{Re}\{U_i^\dagger(x_1+a_4)U_4^\dagger(x_1)U_i(x_1)U_4(x_1+a_i)\}^{mm}+3\Big]\\
&-8\kappa^2\sum_{\vec{x}_1}\Big[\sum_m\mathrm{Im}\{U_4^\dagger(x_1-a_i)U_i(x_1-a_i)U_4(x_1)U_i^\dagger(x_1+a_4-a_i)\}^{mm}\Big]\\
&-8\kappa^2\sum_{\vec{x}_1}\Big[\sum_m\mathrm{Im}\{U_4(x_1-a_4+a_i)U_i^\dagger(x_1)U_4^\dagger(x_1-a_4)U_i(x_1-a_4)\}^{mm}\Big]\\
&-8\kappa^2\sum_{\vec{x}_1}\Big[\sum_m\mathrm{Re}\{U_i(x_1-a_4-a_i)U_4(x_1-a_4)U_i^\dagger(x_1-a_i)\\
&\times U_4^\dagger(x_1-a_4-a_i)\}^{mm}+3\Big]\\
&+8\kappa^2\sum_{\vec{x}_1}\Big[\sum_m\mathrm{Re}\{U_i(x_1-a_4-a_i)U_4(x_1-a_4)U_i^\dagger(x_1-a_i)\\
&\times U_4^\dagger(x_1-a_4-a_i)\}^{mm}+3\Big]\\
&-8\kappa^2\sum_{\vec{x}_1}\Big[\sum_m\mathrm{Im}\{U_4(x_1-a_4+a_i)U_i^\dagger(x_1)U_4^\dagger(x_1-a_4)U_i(x_1-a_4)\}^{mm}\Big]\\
&-8\kappa^2\sum_{\vec{x}_1}\Big[\sum_m\mathrm{Im}\{U_4^\dagger(x_1-a_i)U_i(x_1-a_i)U_4(x_1)U_i^\dagger(x_1+a_4-a_i)\}^{mm}\Big]\\
&-8\kappa^2\sum_{\vec{x}_1}\Big[\sum_m\mathrm{Re}\{U_i^\dagger(x_1+a_4)U_4^\dagger(x_1)U_i(x_1)U_4(x_1+a_i)\}^{mm}+3\Big]\\
=&\frac{1}{24a^2}16\kappa^2\sum_{\vec{x}_1}\Big[\sum_m\mathrm{Im}\{U_4^\dagger(x_1-a_i)U_i(x_1-a_i)U_4(x_1)U_i^\dagger(x_1+a_4-a_i)\}^{mm}\\
&+\sum_m\mathrm{Im}\{U_4(x_1-a_4+a_i)U_i^\dagger(x_1)U_4^\dagger(x_1-a_4)U_i(x_1-a_4)\}^{mm}\Big].
\end{aligned}
\tag{B26}
$$

[1] E. W. Hughes and R. Voss, Annu. Rev. Nucl. Part. Sci. **49**, 303 (1999).
[2] D. H. Beck and R. D. McKeown, Annu. Rev. Nucl. Part. Sci. **51**, 189 (2001).
[3] M. J. Musolf *et al.*, Phys. Rep. **239**, 1 (1994).
[4] D. S. Armstrong *et al.* (G0 Collaboration), Phys. Rev. Lett. **95**, 092001 (2005).
[5] R. D. Young, J. Roche, R. D. Carlini, and A. W. Thomas, Phys. Rev. Lett. **97**, 102002 (2006).
[6] G. Hohler, *Publications of the 8th International Symposium on Meson-Nucleon Physics and the Structure of the Nucleon, 1999* [PiN Newsletter 15, 123 (1999)]; M. Knecht, *Publications of the 8th International Symposium on Meson-Nucleon Physics and the Structure of the Nucleon, 1999* [PiN Newsletter 15, 108 (1999)].
[7] T. Adams *et al.*, Phys. Rev. Lett. **99**, 192001 (2007).
[8] W. K. Tung, H. L. Lai, A. Belyaev, J. Pumplin, D. Stump, and C.-P. Yuan, J. High Energy Phys. 02 (2007) 053.
[9] G. Watt, A. D. Martin, W. J. Stirling, and R. S. Thorne, *Recent Progress in Global PDF Analysis", Proc. of 16th International Workshop on Deep Inelastic Scattering and Related Subjects (DIS'08)* 2008.
[10] G. P. Zeller *et al.*, Phys. Rev. Lett. **88**, 091802 (2002).
[11] A. I. Signal and A. W. Thomas, Phys. Lett. B **191**, 205 (1987).
[12] S. J. Brodsky and B. Q. Ma, Phys. Lett. B **381**, 317 (1996).
[13] F. G. Cao and A. I. Signal, Phys. Lett. B **559**, 229 (2003).
[14] J. Alwall and G. Ingelman, Phys. Rev. D **70**, 111505 (2004).
[15] Y. Ding, R. G. Xu, and B. Q. Ma, Phys. Lett. B **607**, 101 (2005).
[16] B. Q. Ma, Int. J. Mod. Phys. A **21**, 930 (2006).
[17] F. Olness *et al.*, Eur. Phys. J. C **40**, 145 (2005).
[18] D. Mason, Phys. Rev. Lett. **99**, 192001 (2007).
[19] M. E. Peskin and D. V. Schroeder, *An Introduction to Quantum Field Theory*, Reading, USA Addison-Wesley, (1995).
[20] I. Montvay and G. Münster, *Quantum Fields on A Lattice* (Cambridge University Press, Cambridge, England, 1997).
[21] C. Best *et al.*, Phys. Rev. D **56**, 2743 (1997).
[22] Ph. Hägler *et al.*, Phys. Rev. D **68**, 034505 (2003).
[23] A. S. Kronfeld and D. M. Photiadis, Phys. Rev. D **31**, 2939 (1985).
[24] M. Baake *et al.*, J. Math. Phys. (N.Y.) **23**, 944 (1982).
[25] J. Mandula *et al.*, Nucl. Phys. **B228**, 91 (1983).
[26] G. Martinelli and C. T. Sachrajda, Nucl. Phys. **B306**, 865 (1988).
[27] G. Martinelli and C. T. Sachrajda, Nucl. Phys. **B316**, 355 (1989).
[28] S. Capitani and G. Rossi, Nucl. Phys. **B433**, 351 (1995).
[29] G. Beccarini, Nucl. Phys. **B456**, 271 (1995).
[30] B. L. Ioffe, Nucl. Phys. **B188**, 317 (1981).
[31] Y. Chung *et al.*, Nucl. Phys. **B197**, 55 (1982).
[32] D. B. Leinweber, R. W. Woloshyn, and T. Draper, Phys. Rev. D **43**, 1659 (1991).
[33] J. N. Labrenz and S. R. Sharpe, Nucl. Phys. B, Proc. Suppl. **34**, 335 (1994); T. Draper *et al.*, Nucl. Phys. B, Proc. Suppl. **34**, 335 (1994).
[34] T. Bhattacharya *et al.*, Phys. Rev. D **53**, 6486 (1996).
[35] A. C. Kalloniatis *et al.*, *Lattice Hadron Physics, Lecture Notes* (Springer-Verlag, Berlin, 2005).
[36] K. F. Liu, Phys. Rev. D **62**, 074501 (2000).
[37] K. F. Liu and S. J. Dong, Phys. Rev. Lett. **72**, 1790 (1994).
[38] K. F. Liu *et al.*, Phys. Rev. D **59**, 112001 (1999).
[39] W. Wilcox, Nucl. Phys. B, Proc. Suppl. **30**, 491 (1993).
[40] C. W. Bernard, *Gauge Theory on a Lattice*, edited by C. Zachos *et al.* (Argonne National Laboratory, Argonne, IL, 1984), p. 85.
[41] T. Draper, Ph.D. thesis, UMI-84-28507, 1984.
[42] C. W. Bernard, T. Draper, G. Hockney, A. M. Rushton, and A. Soni, Phys. Rev. Lett. **55**, 2770 (1985).
[43] L. Maiani *et al.*, Nucl. Phys. **B293**, 420 (1987).
[44] R. Gupta *et al.*, Phys. Rev. D **44**, 3272 (1991).
[45] S. J. Dong *et al.*, Phys. Rev. Lett. **75**, 2096 (1995).
[46] J. Viehoff *et al.* (SESAM Collaboration), Nucl. Phys. B, Proc. Suppl. **63**, 269 (1998).
[47] N. Mathur *et al.*, Phys. Rev. D **62**, 114504 (2000).
[48] K. F. Liu, S. J. Dong, T. Draper, J. M. Wu, and W. Wilcox, Phys. Rev. D **49**, 4755 (1994).
[49] W. Wilcox *et al.*, Nucl. Phys. B, Proc. Suppl. **119**, 404 (2003).
[50] C. W. Bernard, lectures at TASI '89, Boulder, CO, Jun 4-30, 1989, Published in Boulder ASI 1989:233-292.
[51] T. Draper *et al.*, Nucl. Phys. **B318**, 319 (1989).
[52] N. Mathur and S. J. Dong, Nucl. Phys. B, Proc. Suppl. **119**, 401 (2003).
[53] S. J. Dong and K. F. Liu, Phys. Lett. B **328**, 130 (1994).
[54] S. Bernardson *et al.*, Comput. Phys. Commun. **78**, 256 (1994).
[55] C. Thron, S. J. Dong, K. F. Liu, and H. P. Ying, Phys. Rev. D **57**, 1642 (1998).
[56] M. Göckeler *et al.*, Nucl. Phys. **B472**, 309 (1996).
[57] G. P. Lepage and P. B. Mackenzie, Phys. Rev. D **48**, 2250 (1993).
[58] S. J. Dong *et al.*, Phys. Rev. D **54**, 5496 (1996).
[59] S. Güsken *et al.*, Phys. Lett. B **227**, 266 (1989).
[60] B. Efron, SIAM Rev. **21**, 460 (1979).
[61] B. A. Berg, Comput. Phys. Commun. **69**, 7 (1992).
[62] T. A. DeGrand, Phys. Rev. D **36**, 176 (1987).
[63] C. Detar and J. B. Kogut, Phys. Rev. D **36**, 2828 (1987).
[64] S. Gottlieb *et al.*, Phys. Rev. D **38**, 2245 (1988).
[65] W. Wilcox, Nucl. Phys. B, Proc. Suppl. **63**, 973 (1998).
[66] W. Wilcox *et al.*, Phys. Rev. D **67**, 013003 (2003).
[67] R. M. Woloshyn (private communication).
[68] A. W. Thomas, W. Melnitchouk, and F. M. Steffens, Phys. Rev. Lett. **85**, 2892 (2000).
[69] J. W. Chen and X. Ji, Phys. Lett. B **523**, 107 (2001).
[70] D. Arndt and M. J. Savage, Nucl. Phys. **A697**, 429 (2002).
[71] M. Dorati, T. A. Gail, and T. R. Hemmert, Nucl. Phys. **A798**, 96 (2008).
[72] S. Aoki *et al.* (PACS-CS Collaboration), arXiv:0807.1661.
[73] C. Best *et al.*, 5th International Workshop on Deep Inelastic Scattering and QCD (DIS 97), Chicago, IL, 1997, arXiv:hep-ph/9706502.
[74] M. Göckeler *et al.*, Nucl. Phys. B, Proc. Suppl. **53**, 81 (1997).
[75] M. Göckeler *et al.*, Phys. Rev. D **53**, 2317 (1996).
[76] D. Dolgov *et al.*, Phys. Rev. D **66**, 034506 (2002).
[77] W. Detmold, W. Melnitchouk, J. W. Negele, D. B. Renner, and A. W. Thomas, Phys. Rev. Lett. **87**, 172001 (2001).
[78] Ph. Hägler *et al.*, Phys. Rev. D **77**, 094502 (2008).

[79] Note that the strange quark appears only in the disconnected insertion.
[80] H. L. Lai *et al.* (CTEQ Collaboration), Eur. Phys. J. C **12**, 375 (2000).
[81] T. Ishikawa *et al.* (CP-PACS Collaborations and JLQCD Collaborations), Proc. Sci., LAT2005 (2006) 057.
[82] D. Kadoh *et al.* (PACS-CS Collaboration), Proc. Sci., LAT2007 (2007) 109.
[83] H. L. Lai *et al.*, Phys. Rev. D **51**, 4763 (1995).